The Matrix Element Method and its Application to Measurements of the Top Quark Mass

Frank Fiedler
Johannes Gutenberg University Mainz

Alexander Grohsjean
CEA, Irfu, SPP, Saclay

Petra Haefner
Max Planck Institute Munich

Philipp Schieferdecker
Karlsruhe Institute of Technology (KIT)

The most precise measurements of the top quark mass are based on the Matrix Element method. We present a detailed description of this analysis method, taking the measurements of the top quark mass in final states with one and two charged leptons as concrete examples. In addition, we show how the Matrix Element method is suitable to reduce the dominant systematic uncertainties related to detector effects, by treating the absolute energy scales for b-quark and light-quark jets independently as free parameters in a simultaneous fit together with the top quark mass. While the determination of the light-quark jet energy scale has already been applied in several recent measurements, the separate determination of the absolute b-quark jet energy scale is a novel technique with the prospect of reducing the overall uncertainty on the top quark mass in the final measurements at the Tevatron and in analyses at the LHC experiments. The procedure is tested on Monte Carlo generated events with a realistic detector resolution.

PACS numbers: 02.70.Uu, 14.65.Ha, 29.85.Fj, 12.15.Ff, 13.87-a, 13.38-b

I. INTRODUCTION

The Matrix Element method is unique among the analysis methods used in experimental particle physics because of the direct link it establishes between theory and event reconstruction. Originally developed to minimize the statistical uncertainty in measurements of $t\bar{t}$ events at the Tevatron experiments D0 and CDF [1], it has since been applied with great success to measurements of the top quark mass m_t [2] and also in the discovery of electroweak production of single top quarks [3]. The method can in principle be used for any measurement, with the largest gain compared to cut-based analysis techniques expected for processes involving intermediate resonances and leading to many-particle final states. In general, the Matrix Element method can be used to determine several unknown parameters (theoretical parameters describing the physics processes measured as well as experimental parameters describing the detector response) at the same time in one measurement, thus also allowing for a reduction of systematic uncertainties. This paper presents the analysis method in general and also gives an example of how the determination of such additional parameters can be implemented.

Recent measurements in $t\bar{t}$ events containing one leptonic and one hadronic W decay ("lepton+jets events") already exploit the known W mass to constrain the energy scale for light-quark jets and significantly reduce the main systematic uncertainty of early measurements of the top quark mass. Among the largest remaining systematic uncertainties is the uncertainty on potential differences between the energy scales S_b and S_l for b- and light-quark jets[1]. Without further improvements, it will soon become a limiting uncertainty for those measurements that dominate the world-average value [4]. In this paper we show how together with the top quark mass, a simultaneous additional measurement of the b-quark jet energy scale, which was first proposed in [5] for the lepton+jets channel, can be incorporated naturally in the Matrix Element technique – not only for measurements in the lepton+jets channel, but also in $t\bar{t}$ events with two leptonic W decays ("dilepton events") where the quantities to be measured cannot be reconstructed based on the kinematical information of a single event alone. This study considers the case of the Tevatron (proton-antiproton collisions at a center-of-mass energy of 1.96 TeV) as a concrete example but is applicable to the two LHC experiments ATLAS and CMS as well.

The paper is structured as follows: In Section II, an overview of the Matrix Element method is given. Section III discusses the generation and selection of $t\bar{t}$ events used for the studies described in the further sections. This is followed by a discussion of the implementation of the likelihood calculation for signal and background processes for $t\bar{t}$ measurements in the lepton+jets and dilepton channels in Section IV. We then describe studies of the performance of the new measurement technique, separately for lepton+jets (Section V) and dilepton (Section VI) $t\bar{t}$ events. In Section VII, systematic uncertainties on m_t are addressed, with an emphasis on the effect of events with significant initial- and final-state radiation. Section VIII summarizes the findings and gives an outlook.

II. THE MATRIX ELEMENT METHOD

The Matrix Element method is based on the likelihood L_{sample} to observe a sample of selected events in the detector. The likelihood is obtained directly from the theory prediction for the differential cross-sections of the relevant processes and the detector resolution and is calculated as a function of the assumed values for each of the parameters to be measured. The minimization of $-\ln L_{\text{sample}}$ yields the measurement of the parameters, where the likelihood L_{sample} for the entire event sample is computed as the product of likelihoods to observe each individual event. This is in contrast to most analysis methods used in experimental particle physics, where distributions from observed events in the detector are compared with corresponding distributions obtained from simulated events that have been generated according to theory and then passed through a detector simulation and the same event reconstruction software.

This paper concentrates on the case of the measurement of the top quark mass in lepton+jets and dilepton events at a hadron collider, where the parameters to be measured are the top quark mass m_t, factors S_b and S_l describing the energy scales for b- and light-quark jets relative to the default energy scale[2], and the fraction $f_{t\bar{t}}$ of signal events in the channel under consideration. A comparison of the Matrix Element method with other methods to measure the top quark mass can be found in [4].

---

[1] The quantities S_b and S_l denote scale factors relative to the nominal detector calibration. In the definition of these factors, it is assumed that all experimental corrections to measured jet energies have been applied to the events that enter the analysis, such that S_b and S_l do not depend on quantities like the jet direction or energy. Uncertainties on such dependencies give rise to additional systematic uncertainties of the measurement e. g. of the top quark mass.

[2] In dilepton $t\bar{t}$ events, only b-quark jets occur and thus only S_b is determined. Only one overall scale factor S_b is determined for all b jets; thus for example no distinction is made between b jets with and without a reconstructed muon inside the jet.

A. The Event Likelihood

The sample likelihood L_{sample} for N measured events to have measured properties $x_1, ..., x_N$ can be written as

$$L_{\text{sample}}(x_1, .., x_N;\, \vec{\alpha}, \vec{\beta}, \vec{f}) = \prod_{i=1}^{N} L_{\text{evt}}(x_i;\, \vec{\alpha}, \vec{\beta}, \vec{f})\,, \tag{1}$$

where the symbol $\vec{\alpha}$ denotes assumed values of the physics parameters to be measured, $\vec{\beta}$ stands for parameters describing the detector response that are to be determined, and $\vec{f}$ is defined below. The likelihood $L_{\text{evt}}(x_i;\, \vec{\alpha}, \vec{\beta}, \vec{f})$ to observe event x_i under the assumption of parameter values $\vec{\alpha}$, $\vec{\beta}$, and $\vec{f}$ is given as the linear combination

$$L_{\text{evt}}(x_i;\, \vec{\alpha}, \vec{\beta}, \vec{f}) = \sum_{\text{processes } P} f_P L_P(x_i;\, \vec{\alpha}, \vec{\beta})\ , \tag{2}$$

where the sum is over all individual processes P that could have led to the observed event x_i, $L_P(x_i;\, \vec{\alpha}, \vec{\beta})$ is the likelihood to observe this event under the assumption that it was produced via process P, and f_P denotes the fraction of events from process P in the entire event sample, with $\sum_P f_P = 1$. In total, the physics parameters $\vec{\alpha}$, the detector response described by $\vec{\beta}$, and the event fractions $\vec{f}$ are to be determined simultaneously from the minimization of $-\ln L_{\text{sample}}$.

The likelihood $L_P(x;\, \vec{\alpha}, \vec{\beta})$ in turn is given by the theoretical description of the process and the resolution of the concrete experiment, and is computed as the convolution of the differential partonic cross section with the parton distribution functions of the colliding hadrons and with the detector response. To make the likelihood calculation manageable, simplifying assumptions are introduced. This concerns the description of both the detector response and the physics processes P, where only the dominant ones are considered explicitly, and where the effects of parton shower and hadronization are accounted for with a simple parametrization. Because of these simplifications, the technique has to be calibrated using fully simulated events before applying it in an actual measurement on data. In this paper, a conceptual study is presented. We show how the method can be validated with events that have been generated under the same assumptions as made in the likelihood calculation, which allows to demonstrate that the measurement method as such is unbiased.

In Equation (2), not all likelihoods L_P necessarily depend on all parameter values; e.g. for the measurement of the top quark mass, the likelihood $L_{t\bar{t}}$ depends on the assumed top quark mass, while the likelihoods for an event to be produced via a background process (which by definition does not involve top quark production or decay) do not. Even if a likelihood does depend on a certain parameter, this dependency does not necessarily have to be taken into account explicitly; for example, for the top quark mass measurement it will be shown in Sections V and VI that the dependency of the likelihoods for background processes on the jet energy scales can be neglected without introducing large biases on the top quark mass and energy scale measurements.

B. The Likelihood for one Process

The individual contributions to the likelihood for an observed event x to be produced via a given process P are described in this section. They are visualized schematically in Figure 1 for the example of a lepton+jets $t\bar{t}$ event at the Tevatron. The observed event x, shown at the right, is fixed while integrating over all possible momentum configurations y of final-state particles. The differential cross section for the process is convoluted with the probability for the final-state partons to yield the observed event (transfer function), and with the probability to find initial-state partons of given flavor and momenta inside the colliding proton and antiproton (parton distribution function). All possible assignments of final-state particles to measured objects in the detector are considered by the transfer function. For each partonic final state under consideration, the initial-state parton momenta are determined by energy and momentum conservation.

The likelihood for a final state with n_f partons and given four-momenta y to be produced in the hard-scattering process is proportional to the differential cross section $\mathrm{d}\sigma_P$ of the corresponding process, given by

$$\mathrm{d}\sigma_P(a_1 a_2 \to y;\, \vec{\alpha}) = \frac{(2\pi)^4 |\mathscr{M}_P\,(a_1 a_2 \to y;\, \vec{\alpha})|^2}{\xi_1 \xi_2 s} \mathrm{d}\Phi_{n_f}\ , \tag{3}$$

where $a_1 a_2$ and y stand for the kinematic variables of the partonic initial and final states, respectively. The symbol $\mathscr{M}_P$ denotes the matrix element for this process, s is the center-of-mass energy squared of the collider, ξ_1 and ξ_2 are

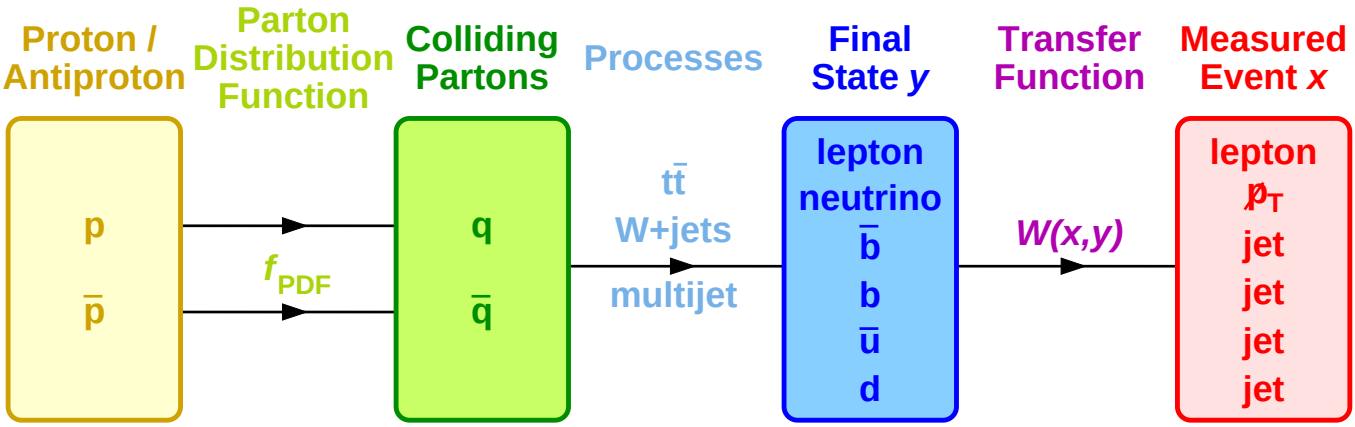

FIG. 1: Schematic representation of the calculation of the likelihood to obtain a given observed lepton+jets event at a proton-antiproton collider (similar figures apply to dilepton events and to other processes).

the momentum fractions of the colliding partons a_1 and a_2 (which are assumed to be massless) within the colliding proton and antiproton[3], and $\mathrm{d}\Phi_{n_f}$ is an element of n_f-body phase space.

To obtain the differential cross section $\mathrm{d}\sigma_P(p\bar{p} \to y;\, \vec{\alpha})$ in $p\bar{p}$ collisions, the differential cross section from Equation (3) is convoluted with the parton density functions (PDF) and summed over all possible flavor compositions of the colliding partons,

$$\mathrm{d}\sigma_P(p\bar{p} \to y;\, \vec{\alpha}) = \int\limits_{\xi_1,\xi_2} \sum_{a_1,a_2} \mathrm{d}\xi_1 \mathrm{d}\xi_2 \; f^{a_1}_{\mathrm{PDF}}(\xi_1) \; \bar{f}^{a_2}_{\mathrm{PDF}}(\xi_2) \; \mathrm{d}\sigma_P(a_1 a_2 \to y;\, \vec{\alpha}) \;, \tag{4}$$

where $f^{a_1}_{\mathrm{PDF}}(\xi_1)$ and $\bar{f}^{a_2}_{\mathrm{PDF}}(\xi_2)$ denote the probability densities to find a parton of given flavor a_1 and momentum fraction ξ_1 in the proton and one of flavor a_2 and momentum fraction ξ_2 in the antiproton, respectively. This equation reflects QCD factorization [6].

The finite detector resolution is taken into account via a convolution with a transfer function $W(x, y;\, \vec{\beta})$ that describes the probability to reconstruct a partonic final state y as x in the detector, given the values $\vec{\beta}$ of the parameters describing the detector response. The differential cross section to observe a given reconstructed event x then becomes

$$\mathrm{d}\sigma_P(p\bar{p} \to x;\, \vec{\alpha}, \vec{\beta}) \;=\; \int\limits_{y} \mathrm{d}\sigma_P(p\bar{p} \to y;\, \vec{\alpha}) \; W(x, y;\, \vec{\beta}) \;. \tag{5}$$

Only events that are inside the detector acceptance and that pass the trigger conditions and offline event selection are used in the measurement. To obtain a properly normalized likelihood, the overall cross section of events observable in the detector,

$$\sigma_P^{\mathrm{obs}}(\vec{\alpha}, \vec{\beta}) = \int\limits_{x,y} \mathrm{d}\sigma_P(p\bar{p} \to y;\, \vec{\alpha}) \; W(x, y;\, \vec{\beta}) \; f_{\mathrm{acc}}(x) \; \mathrm{d}x \;, \tag{6}$$

is used, where $f_{\mathrm{acc}} = 1$ for selected events and $f_{\mathrm{acc}} = 0$ otherwise. One then obtains

$$L_P(x;\, \vec{\alpha}, \vec{\beta}) \; \mathrm{d}x \;=\; \frac{\mathrm{d}\sigma_P(x;\, \vec{\alpha}, \vec{\beta})}{\sigma_P^{\mathrm{obs}}(\vec{\alpha}, \vec{\beta})} \tag{7}$$

as the (differential) likelihood that an event produced via process P has measured properties x (and not other properties that would still lead to an event passing the event selection criteria).

[3] This discussion is based on the situation at the Tevatron $p\bar{p}$ collider as a concrete example but is equally valid for the LHC when the antiproton is replaced with a proton and the appropriate PDF is used.

C. Description of the Detector Response

This section describes a parametrization of the transfer function $W(x, y; \vec{\beta})$ appropriate for measurements of high-p_T objects at a hadron collider. The matrix element method is based on a fast parametrization that reproduces the basic properties of the detector. Any biases introduced can be determined (and then corrected for) when ensemble tests as described in Section II F are performed with events generated with a full detector simulation, typically based on the GEANT [7] package. This section is written with measurements in $t\bar{t}$ events in mind but is applicable to other processes as well.

The transfer function $W(x, y; \vec{\beta})$ describes the probability density $\mathrm{d}P$ to reconstruct an assumed partonic final state y as a measurement x in the detector:

$$\mathrm{d}P = W(x, y; \vec{\beta})\mathrm{d}x \ . \tag{8}$$

Because the final-state partons are assumed to result in some measured event x, the normalization condition

$$\int_x W(x, y; \vec{\beta})\mathrm{d}x = 1 \tag{9}$$

holds, where the integral is over all possible events x. Effects due to selection cuts or finite detector acceptance are discussed in Section II D.

The transfer function is assumed to factorize into contributions from each measured final-state particle. Aspects to be considered in the transfer function are in principle the measurement of the momentum of a particle (both of its energy and of its direction) as well as its identification. Thus b-tagging information for the jets can be included, which can help to distinguish signal from background events.

In many applications like the description of $t\bar{t}$ events, a number of assumptions can be made [8] about how final-state particles are measured in the detector, such that the dimensionality of the integration over the final-state particle phase space described in Section II B is reduced. Individual particles can be described in the transfer function as follows:

- **Isolated energetic electrons:** Electrons are assumed to be unambiguously identified (i.e. an electron is not reconstructed as a muon or a jet). The electron direction and energy are both assumed to be well-measured, i.e. during integration, the final-state electron is assumed to be identical to the measured particle. This is justified for $t\bar{t}$ events since the resolution for electrons is far better than that for jets, and the jet energy resolution will dominate all effects due to the finite detector resolution.
- **Isolated energetic muons:** As for electrons, muons are assumed to be unambiguously identified, and their directions to be precisely measured. However, instead of the energy the detector typically yields a measurement of $(q/p_T)_\mu$, the muon charge divided by the transverse momentum. Consequently, the muon energy resolution can be poor for high-p_T muons, and thus a transfer function W_μ allowing for a finite resolution is introduced. In the studies presented in this paper, the function

  $$W_\mu\left((q/p_T)_\mu^{\mathrm{rec}}, (q/p_T)_\mu^{\mathrm{mat}}\right) = \frac{1}{\sqrt{2\pi}\sigma}\exp\left(-\frac{1}{2}\left(\frac{(q/p_T)_\mu^{\mathrm{rec}} - (q/p_T)_\mu^{\mathrm{mat}}}{\sigma}\right)^2\right) \tag{10}$$

  is used to describe the likelihood that a muon with charge and momentum $(q/p_T)_\mu^{\mathrm{mat}}$ (described by the *mat*rix element) is *rec*onstructed with $(q/p_T)_\mu^{\mathrm{rec}}$. The resolution σ depends on the pseudorapidity η to account for muon tracks at large $|\eta|$ that do not reach the full radius of the tracking detector. The parameter values are taken from [8].
- **Energetic τ leptons:** Events with energetic τ lepton decays are typically selected if the visible decay products pass a minimum energy cut. In this case, the directions of the visible decay products are close to that of the original τ lepton, but only a fraction of the τ energy can be measured in the detector.
  In this paper, only leptonic decays $\tau \to \ell\overline{\nu}_\ell\nu_\tau$ are considered, where the symbol ℓ denotes an electron or muon. Consequently, a transfer function $W_\tau\left(E_\ell^{\mathrm{rec}}/E_\tau^{\mathrm{mat}}\right)$ is introduced to describe the likelihood to obtain a charged lepton with a given energy fraction E_ℓ/E_τ of the decaying τ lepton. For the study presented here, it is parametrized as a 3^{rd}-order polynomial as shown in Figure 2. The τ direction is taken to be well approximated by the direction of the reconstructed charged lepton.
  For muonic τ decays, the muon transfer function introduced above in principle has to be taken into account as well to describe the transition from the assumed to the reconstructed muon transverse momentum. However, muons from τ decays typically have low enough transverse momenta so that the muon p_T can be assumed to be well-measured in most applications. In the following, the muon transfer function is omitted for muonic τ decays. Also, in this study we consider the reconstruction efficiency to be independent of the lepton energy.

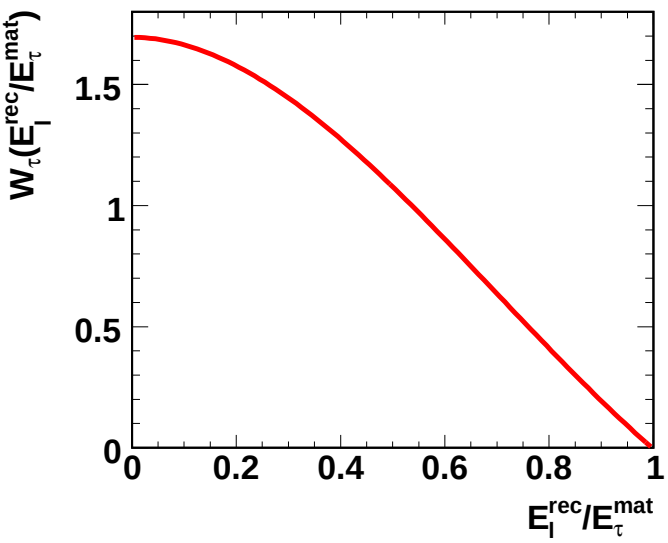

FIG. 2: Likelihood for an electron or muon to carry a given energy fraction of the initial τ lepton energy.

- **Energetic quarks and gluons:** The directions of final-state quarks and gluons are assumed to be well-measured by the jet directions, and transfer functions are introduced for the jet energy measurement. The probability density for a jet energy measurement $E_j^{\rm rec}$ in the detector if the true quark energy is $E_j^{\rm mat}$ (depending on the overall jet energy scale S_b or S_l) is given by the jet energy transfer function $W_{\rm jet}\left(E_j^{\rm rec},\ E_j^{\rm mat},\ \phi_j^{\rm mat};\ S_\phi\right)$. In principle, different transfer functions apply to gluon jets and jets from different quark flavors $\phi_j^{\rm mat}$.
For $S_\phi \neq 1$, the jet transfer function is computed as

$$W_{\rm jet}(E_j^{\rm rec}, E_{j'}^{\rm mat}, \phi_{j'}^{\rm mat};\ S_\phi) = \frac{W_{\rm jet}(\frac{E_j^{\rm rec}}{S_\phi}, E_{j'}^{\rm mat}, \phi_{j'}^{\rm mat};\ 1)}{S_\phi}\ , \tag{11}$$

where the factor S_ϕ in the denominator ensures the correct normalization in the absence of selection cuts.
In this paper, the same jet energy transfer function is used to describe light-quark (u, d, s, and c) and gluon jets[4]; an independent transfer function is used for b-quark jets. The parametrization of the transfer function follows that of the D0 experiment given in [8], with parameters depending on the jet energy and pseudorapidity. In a fraction of those b jets that contain a semimuonic b-hadron decay, the muon is identified, and these jets could in principle be described with a separate transfer function [8] (while the jets with unidentified semileptonic decays would still have to be described with one function together with all other b jets). In this paper, only one class of b jets is considered, because the focus is to show how an energy scale for b jets can be determined at all, and only one overall energy scale factor S_b is determined for b jets. Once this is achieved, it will be possible in principle to determine two independent energy scales for the different classes of reconstructed b jets.
The ability of the detector to distinguish quarks from gluons and to identify the quark flavor is limited. Nevertheless, identification of b-quarks (b-tagging) can be useful to distinguish signal and background events, or to identify the correct assignment of final-state quarks to measured jets in final states like lepton+jets $t\bar{t}$ events that contain both light and b-quark jets. In this paper, we follow the approach introduced in [9] to include a term W_b in the transfer function which describes the likelihood for parton j with assumed flavor $\phi_j^{\rm mat}$ to be reconstructed with b-tagging information $\mathcal{B}_j^{\rm rec}$. If b tagging is used as a binary decision, then one simply has

$$W_b\left(\mathcal{B}_j^{\rm rec},\ \phi_j^{\rm mat}\right) = \begin{cases} \epsilon_b\left(\phi_j^{\rm mat}\right) & \text{if the jet } j \text{ is } b\text{-tagged and} \\ 1-\epsilon_b\left(\phi_j^{\rm mat}\right) & \text{otherwise,} \end{cases} \tag{12}$$

[4] In events passing the $t\bar{t}$ selection cuts, gluon jets arise in background processes whose description is anyway only approximate; therefore no separate transfer function for gluon jets is introduced.

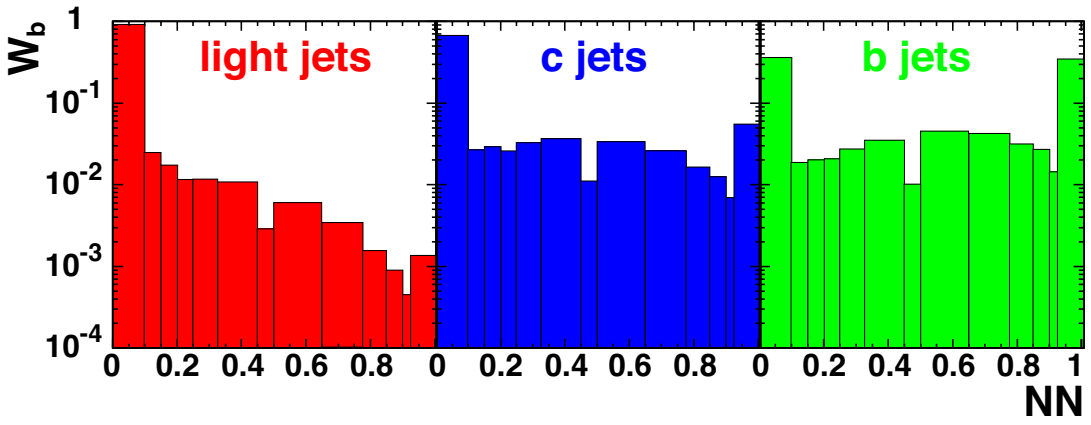

FIG. 3: The function W_b used to parametrize the b-tagging performance. The likelihood W_b for a jet to be reconstructed as b-tagged with given b-tagging output $\mathcal{B}^{\rm rec}$ is shown for light, c-quark, and b-quark jets. In this paper, the output NN of an artificial neural network used in the D0 experiment [10] is taken as a concrete example. The first bin contains jets that fail the b-tagging preselection. The structure in the histogram is due to the non-equidistant binning.

where $\epsilon_b\,(\phi)$ is the b-tagging efficiency for a jet from a parton of flavor ϕ.
Typically, b-tagging algorithms yield a continuous output (for example, the decay length significance of a secondary vertex within a jet, or the output of an artificial neural network). Instead of a binary decision, the quantity W_b can be parametrized as a function of this continuous value. Such an approach naturally makes optimal use of the information. As a compromise, it is possible to use several (rather than only two) bins in the output value. This is the concept used in this publication. Figure 3 shows the values W_b for jets in lepton+jets $t\bar{t}$ events as used in the study presented here, which corresponds to the b-tagging performance of the D0 experiment [10]. For the study in this paper, the W_b functions are assumed not to depend on the jet transverse momentum or pseudorapidity, but this will be a straightforward extension of the method for future measurements.

- **Energetic neutrinos:** Neutrinos are not measured in the detector, but still an integration has to be performed over assumed values for all momentum components of all final-state neutrinos in an event. Information on neutrino momenta can be partly inferred from mass constraints (e.g., m_W or m_t in $t\bar{t}$ events). The additional assumption is made in this paper that events are balanced in the transverse plane, i.e. that the $t\bar{t}$ system has zero transverse momentum. This assumption is dropped in Section VII A, which means that an integration over two additional variables has to be carried out.
  The presence of neutrinos in an event is typically inferred from an imbalance in the transverse plane (non-zero missing transverse momentum $\not\!\!\vec{p}_T$). It is not straightforward to parametrize the resolutions of the two $\not\!\!\vec{p}_T$ components since they depend on the resolutions of all other reconstructed objects in the event. Instead, the vector sum of transverse momenta of all reconstructed objects that are not assigned to the final state in question could be considered. In the case of $t\bar{t}$ events at the Tevatron, this would be calorimeter measurements outside of the jets assigned to the $t\bar{t}$ final state. In this paper, however, as in [8], no corresponding transfer function factor is introduced.

In addition to the detector resolution, one has to take into account the fact that the particles measured in the detector cannot be assigned unambiguously to specific final-state particles. Consequently, all possibilities must be considered, and their contributions to the transfer function summed.

The total transfer function can be written as

$$
\begin{aligned}
W(x,y;\,S_b,S_l) \;=\; \sum_{i=1}^{n_{\mathrm{comb}}} \; & \prod_{e=1}^{n_e} \delta^{(3)}\left(\vec{p}_e^{\,\mathrm{rec}} - \vec{p}_{e'}^{\,\mathrm{mat}}\right) \times \\
& \prod_{m=1}^{n_\mu} \delta^{(2)}\left(\vec{u}_\mu^{\,\mathrm{rec}} - \vec{u}_{\mu'}^{\,\mathrm{mat}}\right) W_\mu\left((q/p_T)_\mu^{\mathrm{rec}}, (q/p_T)_{\mu'}^{\mathrm{mat}}\right) \times \\
& \prod_{t=1}^{n_\tau} \delta^{(2)}\left(\vec{u}_\ell^{\,\mathrm{rec}} - \vec{u}_{\tau'}^{\,\mathrm{mat}}\right) W_\tau\left(E_\ell^{\mathrm{rec}}/E_{\tau'}^{\mathrm{mat}}\right) \times \\
& \prod_{j=1}^{n_j} \delta^{(2)}\left(\vec{u}_j^{\,\mathrm{rec}} - \vec{u}_{j'}^{\,\mathrm{mat}}\right) W_{\mathrm{jet}}\left(E_j^{\mathrm{rec}},\; E_{j'}^{\mathrm{mat}},\; \phi_{j'}^{\mathrm{mat}};\; S_\phi\right) W_b\left(\mathcal{B}_j^{\mathrm{rec}},\; \phi_{j'}^{\mathrm{mat}}\right) \;,
\end{aligned}
\tag{13}
$$

where the four lines represent the contributions from electrons, muons, tau leptons, and jets, respectively. It is understood that a term only appears if the corresponding particle is present in the final state under consideration. The number of possible assignments of reconstructed ("rec") particles to final-state particles in the process described by the matrix element ("mat") is denoted by n_{comb}, and i stands for one specific permutation. The symbols n_e, n_μ, n_τ, and n_j stand for the numbers of electrons, muons, tau leptons, and quarks or gluons in the final state. A reconstructed particle is denoted by e, m, t, or j. The symbols e', m', t', and j' stand for the corresponding final-state particle assumed in the matrix element integration, which is given by the index i of the permutation and the index of the reconstructed particle: $e' = e'_{i,\,e}$ (and accordingly for muons, tau leptons, and jets). The flavor $\phi_{j'}^{\mathrm{mat}}$ of final-state parton j' assigned to jet j is given by the permutation i. The jet energy scale appropriate for jet j (S_b or S_l) is denoted by S_ϕ and selected according to the assumed flavour $\phi_{j'}^{\mathrm{mat}}$. The symbol $\mathcal{B}_j^{\mathrm{rec}}$ stands for any output from a b-tagging algorithm.

Because of the assumption that the transfer function factorizes into independent contributions from the final-state particles, it may in principle also depend on $\vec{\alpha}$. For example, in a top quark mass measurement, smaller top quark masses correspond to a smaller mean angular separation of jets, which may lead to a broadening of the jet energy resolution. Such effects are however typically small and are therefore neglected in the simplified description of the detector response with transfer functions; they would implicitly be taken into account in a calibration of the measurement with fully simulated events.

D. Normalization of the Likelihood

The normalization condition for the likelihood L_P for each process is given by

$$
\int_x L_P(x;\,\vec{\alpha},\vec{\beta})\; f_{\mathrm{acc}}(x)\; \mathrm{d}x = 1\,, \tag{14}
$$

where the inclusion of the factor $f_{\mathrm{acc}}(x)$ is equivalent to integrating only over those configurations x of observed events that pass the event selection criteria. The normalization condition is fulfilled according to the definition of the observable cross section σ_P^{obs} in Equation (6). The calculation of σ_P^{obs} is intimately related with the normalization of the transfer function. Both aspects are discussed in this section.

1. *Normalization of the Jet Energy Transfer Function*

The normalization condition of the jet energy transfer function used in previous implementations of the Matrix Element method [8, 9] is given by

$$
\int_{E_j^{\mathrm{rec}}>0} W_{\mathrm{jet}}(E_j^{\mathrm{rec}}, E_{j'}^{\mathrm{mat}}, \phi_{j'}^{\mathrm{mat}};\; S_\phi)\, \mathrm{d}E_j^{\mathrm{rec}} = 1\;. \tag{15}
$$

We call this a *process-based* normalization scheme as it reflects the concept that a final-state quark or gluon gives rise to a jet of any energy (or is not reconstructed as a jet if the energy is below the jet reconstruction threshold of the experiment); thus this normalization scheme does not depend on the event selection cuts. A modified, *selection-based*

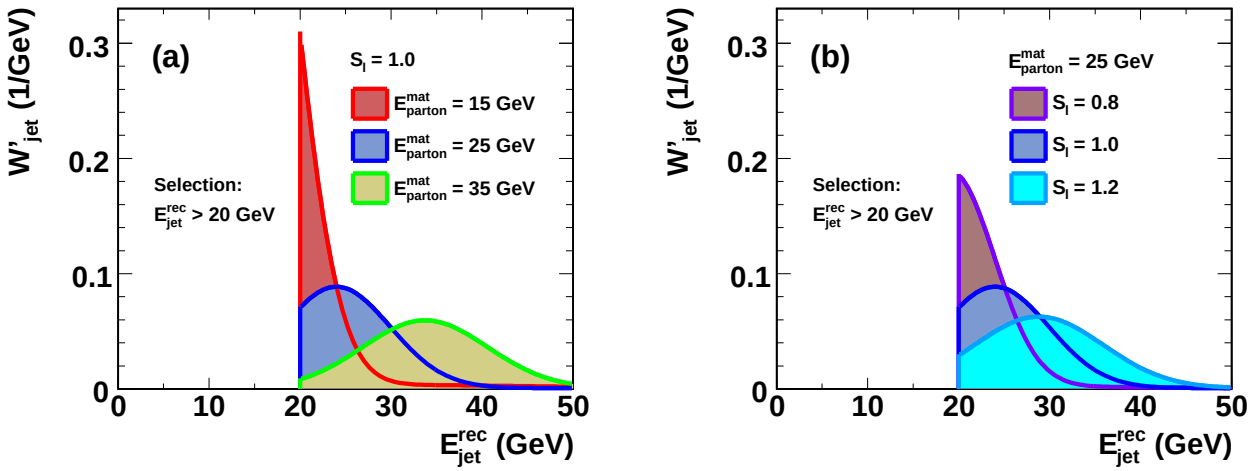

FIG. 4: Jet energy transfer function W'_{jet} in the modified normalization scheme. Plot (a) shows the transfer functions for light-quark jets at $\eta = 0$ for an assumed value of $S_l = 1.0$ and assumed parton energies of 15 GeV (red), 25 GeV (blue), and 35 GeV (green line). Plot (b) shows the same transfer function for different assumed S_l values (violet: $S_l = 0.8$, blue: $S_l = 1.0$, and cyan: $S_l = 1.2$) and an assumed parton energy of 25 GeV.

normalization scheme which simplifies the computation of the normalization integral given in Equation (6) but leaves the likelihood L_P unchanged is introduced in this section.

We assume that the event selection requires a reconstructed object for every charged lepton and every quark or gluon in the final state (this means for example that the presence of four jets is required for lepton+jets $t\bar{t}$ events), and that the jet selection cuts are identical for all jets. The selection-based normalization of the transfer function is based on the concept that events only enter the analysis if all these reconstructed objects pass the corresponding selection criteria. This means that every possible partonic final state in the integral in Equation (5) is assumed to yield an observed event that passed the event selection. Thus, a modified jet energy transfer function W'_{jet} is introduced in the top quark mass measurement, which satisfies the condition

$$\int\limits_{E_j^{\text{rec}} > E_{\text{cut}}(|\eta_j|)} W'_{\text{jet}}(E_j^{\text{rec}}, E_{j'}^{\text{mat}}, \phi_{j'}^{\text{mat}};\ S_\phi)\, \mathrm{d}E_j^{\text{rec}} = 1\ , \tag{16}$$

i.e. the parton under consideration is assumed to have led to a jet that passed the selection cut $E_j^{\text{rec}} > E_{\text{cut}}$, where the energy cut normally depends on the polar angle of the jet since a transverse energy cut is used in the event selection. Equation (16) ensures that in Equation (6),

$$\int\limits_x W'(x, y;\ \vec{\beta}) f_{\text{acc}}(x) \mathrm{d}x = 1\ . \tag{17}$$

It is shown in Section II D 3 that the modified denominator $\sigma_P^{\text{obs}\prime}$ which is then needed in Equation (7) to compute the likelihood L_P becomes independent of the parameters $\vec{\beta}$ that describe the detector response.

The effect of this selection-based normalization scheme on the jet energy transfer function W'_{jet} is shown in Figure 4(a) for the double-Gaussian function used in this study: If the parton energy is assumed to be very small, then a small reconstructed jet energy just above the cut value is most likely. However, the function is still normalized to unit area as it is assumed that the parton must have given rise to a jet that passed the selection cut (in this example set at $E > 20$ GeV corresponding to $\eta = 0$ for the event selection criteria of Section III). The dependence of the jet energy transfer function on the parameters $\vec{\beta}$ that describe the detector response must also be accounted for as explained in Figure 4(b): For every S_l hypothesis the same event sample is considered in the measurement, and therefore the event selection (in this example the minimum jet transverse energy cut) cannot depend on the assumed S_l value. For different assumed values of S_l, the W'_{jet} curve varies, and the normalization of the curve must be adjusted to ensure that the normalization condition in Equation (16) is satisfied.

2. Normalization of the Muon and τ Transfer Functions

It is assumed that every τ lepton decays to an electron or muon that passed the event selection. The τ energy has to be larger than the energy of the reconstructed lepton. Consequently, the selection-based normalization condition is

$$\int\limits_{E_\ell^{\mathrm{rec}} > E_{\mathrm{cut}}(|\eta_\ell|)}^{E_\ell^{\mathrm{rec}} < E_{\tau'}^{\mathrm{mat}}} W'_\tau \left(\frac{E_\ell^{\mathrm{rec}}}{E_{\tau'}^{\mathrm{mat}}} \right) \mathrm{d}\left(\frac{E_\ell^{\mathrm{rec}}}{E_{\tau'}^{\mathrm{mat}}} \right) \;=\; 1\,. \tag{18}$$

Because of the non-zero lower integration bound the transfer function W_τ has to be scaled with an appropriate overall factor that depends on the reconstructed lepton energy and pseudorapidity to arrive at the modified function W'_τ.

In comparison with the jet energy resolution, the muon transverse momentum resolution is good for muons close to the minimum transverse momentum cut, and only a negligible fraction of muons is affected by this cut. In addition, it is assumed that final-state muons passing the selection cuts are always reconstructed as muons. Thus, a calculation of the normalization corresponding to Equation (18) can be omitted for muons.

3. Observable Cross Section

To derive the denominator $\sigma_P^{\mathrm{obs}\prime}$ with which to normalize the likelihood L_P for a given process P, it follows from Equations (14), (7), and (5) that

$$\begin{aligned}
&\frac{1}{\sigma_P^{\mathrm{obs}\prime}} \int\limits_x \int\limits_y \mathrm{d}\sigma_P(p\bar{p} \to y;\, \vec{\alpha})\; W'(x, y;\, \vec{\beta})\; f_{\mathrm{acc}}(x)\; \mathrm{d}x \;=\; 1 \\
\Leftrightarrow\; &\frac{1}{\sigma_P^{\mathrm{obs}\prime}} \int\limits_y \mathrm{d}\sigma_P(p\bar{p} \to y;\, \vec{\alpha}) \int\limits_x W'(x, y;\, \vec{\beta})\; f_{\mathrm{acc}}(x)\; \mathrm{d}x \;=\; 1 \\
&\Leftrightarrow \int\limits_y \mathrm{d}\sigma_P(p\bar{p} \to y;\, \vec{\alpha}) \;=\; \sigma_P^{\mathrm{obs}\prime}\,,
\end{aligned} \tag{19}$$

where the normalization condition for the modified transfer function W' (Equation (17)) has been used in the last step. The quantity $\sigma_P^{\mathrm{obs}\prime}$ is thus only a function of the physics parameters $\vec{\alpha}$, but not of the detector performance parameters $\vec{\beta}$.

In the definition of $\sigma_P^{\mathrm{obs}\prime}$, the integral over the observed events x is not over the full phase space, but instead only over that part of the phase space that passes the kinematic event selection. Typically, regions of small jet transverse energy E_T or large $|\eta|$ will be excluded from the integration region.

Because the normalization of the jet energy transfer function W'_{jet} described in Section II D 1 accounts for the lower jet E_T cut, any jet energy scale dependence of $\sigma_P^{\mathrm{obs}\prime}$ is eliminated. In contrast, the jet angular resolution is approximated with a δ function to save integration time, and this means that the integration over y must exclude those angular regions that do not pass the event selection. Through the angular acceptance cuts (and through the matrix element $\mathcal{M}_P$ itself, of course), $\sigma_P^{\mathrm{obs}\prime}$ still depends on the physics parameters $\vec{\alpha}$. A similar argument holds for angular acceptance cuts in the charged lepton selection.

The above argument is only valid if the normalization condition of Equation (17) is fulfilled for the modified transfer function W'. In practice, this is difficult to implement for event selection cuts based on quantities that depend on more than one reconstructed particle. For example, the $\not\!\!p_T$ cut in Section III does not fulfill this criterion since it depends on all measured final-state particles. Therefore, an S_b dependence of $\sigma^{\mathrm{obs}\prime}$ is taken into account in the analysis of dilepton $t\bar{t}$ events described in Section VI. For the measurement with lepton+jets events, it is shown in Section V that the S_b and S_l dependence of $\sigma^{\mathrm{obs}\prime}$ can be neglected for the less stringent $\not\!\!p_T$ cut applied in the event selection.

4. Process-Based Normalization Scheme

It is possible to choose a process-based transfer function normalization according to Equation (15). In this case, the dependency of the transfer function normalization on the parameters $\vec{\beta}$ describing the detector resolution is not

taken into account. This means that in the last step of the derivation in Equation (19), a dependency on $\vec{\beta}$ remains and $\sigma_P^{\rm obs}$ has to vary as a function of both $\vec{\alpha}$ and $\vec{\beta}$.

This process-based scheme has the advantage that the transfer function W accomodates the possibility of jets not passing the selection cuts. For analyses like m_t measurements in $t\bar{t}$ events as described in this paper, the number of jets required in the event selection ensures that in any event where this is the case an additional hard parton would have to be produced which yields a jet passing the cuts. In principle, such events have to be described by the signal process. At the Tevatron their contribution to the event sample is so small that they do not have to be accounted for explicitly in the method until the final calibration step. Consequently, the selection-based transfer function normalization described in Sections II D 1 and II D 2 is chosen for the studies described in this paper, as it eliminates the dependency of $\sigma^{\rm obs'}$ on the parameters $\vec{\beta}$ and thus facilitates the simultaneous measurement of several parameters. This picture may change for measurements in $t\bar{t}$ events at the LHC, where initial-state radiation becomes much more relevant.

5. *Normalization of the Background Likelihood*

The normalization of the likelihoods can in principle be determined in the same way for all processes considered. Alternatively, if the normalization of the likelihood L_{P_0} for one specific process P_0 (for example, the signal process) has been determined as described above and if the fraction f_{P_0} of events from that process in the selected sample is left as a free parameter in the analysis, it is possible to relate the absolute normalization of the likelihoods for all other processes to that of process P_0. One can then make use of the fact that the fit described in Section II E will yield a signal fraction f_{P_0} of the sample that is too small if the background likelihood is too large and vice versa, and one can adjust the relative normalization in the validation of the Matrix Element method until the signal fraction is determined correctly. This concept can only be applied if the cross-section for the process P_0 is well-known (like for example for $t\bar{t}$ production). It is then helpful in particular if the likelihoods for background processes as implemented in the analysis do not depend on any of the parameters $\vec{\alpha}$ and $\vec{\beta}$: In such a case, only one normalization constant needs to be determined for each background process.

E. Fitting Procedure

For a given sample of selected events, the parameters to be measured are determined as those values that maximize the likelihood $L_{\rm sample}$. One wants to determine n_α physics parameters, n_β parameters describing the detector resolution, and n_{f_P} fractions of events from different processes P. For every measured event, the likelihoods for each process are calculated for an $(n_\alpha + n_\beta)$-dimensional grid of assumed parameter values. Given these grids of likelihood values for each process, the sample likelihood $L_{\rm sample}(x_1, .., x_N; \vec{\alpha}, \vec{\beta}, \vec{f})$ defined in Equation (1) is available for an $(n_\alpha + n_\beta + n_{f_P})$-dimensional grid of assumed parameter values.

The measurement value of a given parameter a and the corresponding uncertainty are then determined from a one-dimensional likelihood $L^{\rm 1d}_{\rm sample}(a)$. The value of $L^{\rm 1d}_{\rm sample}(a)$ is obtained by marginalization of all other parameters; in practice, this is done by keeping the value of a constant, varying the assumed values of all $(n_\alpha + n_\beta + n_{f_P} - 1)$ other parameters, and taking the maximum $L_{\rm sample}$ value. The one-dimensional function $-\ln L^{\rm 1d}_{\rm sample}(a)$ is fitted with a parabola. The parameter value that minimizes the parabola is taken to be the measurement value, and the measurement uncertainty is given by the parameter values where the fitted parabola rises by $+\frac{1}{2}$ above the minimum. By construction, this procedure takes correlations between the parameters into account.

F. Validation With Ensemble Tests

To validate the measurement technique, tests are performed with simulated events generated under the assumptions used in the Matrix Element method, i. e. using the same PDF set, matrix element, and transfer function. A pseudo-experiment emulates a measurement performed on data and consists of events randomly drawn from Monte Carlo event pools for signal and background processes. The numbers of events taken from the different pools are chosen to reflect the fractions observed in the data. An ensemble of several pseudo-experiments is performed for each of a number of sets of assumed input parameter values. The range of assumed values is chosen according to previous determinations and the expected precision of the measurement.

Taking the results from all ensembles, the following information is obtained:

- The relation between the expected (mean) measurement values and the corresponding true input values. It is expected that the method yields unbiased results if the Matrix Element method reflects the properties of the events.
- The distribution of measurement uncertainties as a function of input parameter values.
- The width w of the pull distribution. To test that the fitted uncertainties describe the actual measurement uncertainty, the deviation of the measurement value from the true value is divided by the fitted measurement uncertainty in each pseudo-experiment. The width of this distribution of deviations normalized by the measurement uncertainties is referred to as *pull width*. It is expected that $w = 1$ if all features of the events are accommodated in the method.

In a similar way, ensemble tests based on fully simulated events can be used to determine any correction of measurement values and fit uncertainties needed when applying the method (which is based on a simplified detector model) to real data.

Because the computation of likelihoods is time-consuming, the size of the pools of simulated events is usually limited and individual events are allowed to be redrawn, i.e. to appear several times even in the same pseudo-experiment. This technique maximizes the information about the expected uncertainties and pull widths, but it has to be taken into account when evaluating the uncertainties of the ensemble test results [11].

To summarize, the validation tests described in Sections V and VI each comprise the three following steps:

1. Likelihood Fit: build one pseudo-experiment and determine $\vec{\alpha}$, $\vec{\beta}$ and $\vec{f}$ (cf. Section II E);
2. Ensemble Test: repeat Step 1 with 1000 pseudo-experiments and obtain mean results, expected uncertainties, and pull widths; and
3. Validation: repeat Step 2 for several input parameter values to obtain calibration curves.

III. SIMULATION AND SELECTION OF $t\bar{t}$ EVENTS

As an example for a concrete implementation of the Matrix Element method described previously, the measurement of the top quark mass in lepton+jets and dilepton $t\bar{t}$ events is described in this and the following sections. The discussion of dilepton events is restricted to events containing one electronic and one muonic W decay, which yield the most precise top quark mass measurement in dilepton events. This section summarizes the generation of smeared events to study the top quark mass measurement and introduces the event selection criteria.

The characteristics of lepton+jets $t\bar{t}$ events at a hadron collider are the presence of one energetic isolated charged lepton, at least four energetic jets (two of which are b-quark jets), and missing transverse momentum due to the unreconstructed neutrino. The main background is from events where a leptonically decaying W is produced in association with four or more jets. Multijet background where one jet mimicks an isolated charged lepton can also enter the event sample.

Dilepton $t\bar{t}$ events are characterized by two oppositely charged energetic isolated leptons (in the case considered here, one electron and one muon), two energetic b-quark jets, and missing transverse momentum due to the two neutrinos from the W decays. The largest physics background in the $e\mu$ channel is from events with $Z \to \tau^+\tau^-$ decays where the Z boson is produced in association with two or more jets; another background channel is the production of two leptonically decaying W bosons together with two jets. Instrumental background arises from events where a leptonically decaying W is produced in association with three or more jets, one of which is misidentified as the second isolated charged lepton.

In principle, events with leptonically decaying τ leptons from W decay contribute to both the lepton+jets and dilepton event samples. However, because of lower transverse momentum or transverse energy cuts on the charged lepton(s) in the event selection (see below), these contributions are typically small. Thus, $t\bar{t}$ events including leptonic τ decays are not simulated for the study presented here (whereas in a real measurement, the effect of such decays has to be accounted for).

For the study presented here, events containing a $q\bar{q} \to t\bar{t}$ reaction in a $p\bar{p}$ collision at 1.96 TeV center-of-mass energy are simulated with the MADGRAPH [12] generator. Events are generated for each of the different top quark masses, varied between 160 GeV and 180 GeV in steps of 5 GeV. The ALPGEN [13] program is used to generate events containing a leptonic W or Z decay in association with additional light partons; events with b quarks are simulated by smearing the light partons with the transfer function for b jets. To simulate the decay of a τ lepton to an electron or muon in $Z/\gamma^*(\to \tau^+\tau^-)jj$ events, the τ transfer function shown in Figure 2 is applied, while the direction of the lepton is left unchanged. For the modeling of the parton distribution functions, the leading-order PDF CTEQ5L [14] is chosen. Multijet background without leptonic W or Z decay is not simulated because it was shown in [8] that

its effect on the measurement in the lepton+jets channel is similar to that of additional W+jets background[5]. All simulated events are passed through the parametrized detector simulation discussed in Section II C, which describes the response of the D0 detector [8]. No simulation of the parton shower and hadronization is performed since the transfer functions account for their effects in addition to the detector resolution. Samples with different true values of S_l are obtained by scaling the smeared light-quark jet energies; values of S_l between 0.9 and 1.1 in steps of 0.05 are used. Similarly, b-quark jets are scaled by S_b, with S_b varied between 0.8 and 1.2 in steps of 0.1, to obtain samples for different true b-jet energy scales. As the S_b constraint is weaker than the S_l one a wider range of generated values was studied for this observable. The association of final-state partons to jets is not assumed to be known in the subsequent analysis. The reconstructed missing transverse momentum $\not\!\!\vec{p}_T$ is taken to be the negative vector sum of all other reconstructed transverse momenta (i.e., after the smearing and scaling described above); this means that before smearing and scaling the $t\bar{t}$ system has zero p_T.

Typical event selection criteria as used by the Tevatron experiments are then applied to the smeared events. Candidate lepton+jets events are required to contain

- one charged lepton within a pseudorapidity range of $|\eta| < 1.1$ (electrons) or $|\eta| < 2.0$ (muons) and with a transverse energy or momentum of at least 20 GeV,
- four jets within $|\eta| < 2.5$ and with (scaled) transverse energies of $E_T > 20\,\text{GeV}$, and
- missing transverse momentum with magnitude $\not\!\!p_T \equiv |\not\!\!\vec{p}_T| > 20\,\text{GeV}$.

The angular separation between the charged lepton and any jet is required to be $\Delta\mathcal{R} \equiv \sqrt{(\Delta\eta)^2 + (\Delta\phi)^2} > 0.5$, and similarly, any jet-jet pair has to be separated by $\Delta\mathcal{R} > 1.0$. No b-tagging requirements for the jets are included, but b-tagging information is used later in the analysis.

Similarly, dilepton events must contain

- one electron and one muon of opposite charges within pseudorapidity ranges of $|\eta| < 1.1$ or $1.5 < |\eta| < 2.5$ (electrons)[6] or $|\eta| < 2.0$ (muons) and with a transverse energy or momentum of at least 15 GeV,
- two jets within $|\eta| < 2.5$ and with (scaled) transverse energies of $E_T > 20\,\text{GeV}$, and
- missing transverse momentum with magnitude $\not\!\!p_T > 30\,\text{GeV}$.

The same $\Delta\mathcal{R}$ separation cuts as above are applied, and in addition the two charged leptons are required to be separated by $\Delta\mathcal{R} > 0.5$.

The event samples described here are used for validating the measurement technique as discussed in Sections V and VI. While the exact event selection criteria are not critical to the method, it is mandatory to adjust the likelihood calculation accordingly.

IV. LIKELIHOOD IMPLEMENTATION FOR MEASUREMENTS IN $t\bar{t}$ EVENTS

This section describes the calculation of the signal and background likelihoods for lepton+jets and dilepton $t\bar{t}$ events. When the likelihood for a certain process has to be evaluated for many hypotheses, a dedicated implementation of the matrix element optimized for speed is beneficial, and it is helpful to limit the number of evaluations of the transfer function. Section IV A discusses the evaluation of the signal $t\bar{t}$ likelihoods for a top quark mass measurement (in the lepton+jets or dilepton channel) as an example for such a case. In contrast, when the number of hypotheses is smaller and/or there are many individual diagrams contributing to a process, interfacing to routines from existing Monte Carlo generators is a powerful solution. Such a case is the evaluation of the background likelihoods for an m_t measurement, which is described in Section IV B. An overview of the event likelihood calculation for the different decay channels and processes in a top quark mass measurement is given in Table I.

channel	processes	likelihoods	parameters
lepton+jets	$q\bar{q} \to t\bar{t}$	$L_{t\bar{t}}$	m_t, S_b, S_l
	$Wjjjj$	L_{Wjjjj}	–
dilepton	$q\bar{q} \to t\bar{t}$	$L_{t\bar{t}}$	m_t, S_b
($e\mu$ channel)	$Z/\gamma^*(\to \tau^+\tau^-)jj$	L_{Zjj}	–

[5] In a real measurement, it is thus possible to model both W+jets and multijet background by the W+jets process to calculate the likelihood L_{sample}, and to account for any differences between W+jets and multijet background when calibrating the measurement using full simulation.

[6] This cut rejects electrons in the transition region between the barrel and endcap parts of the electromagnetic calorimeter, which has poor electron identification performance and is typically located at around $1.1 < |\eta| < 1.5$.

TABLE I: Overview of the $L_{\rm evt}$ calculation in the lepton+jets and dilepton channels. The column entitled "processes" lists the signal and background processes taken into account in the calculation of the event likelihood $L_{\rm evt}$. The symbol "j" refers to any light parton, i.e. a u, d, s, or c quark (or antiquark) or a gluon. The rightmost column shows the parameters on which the likelihoods L_P for each individual process depend. In principle the background likelihoods depend on S_l, but as shown later in the paper it is possible to omit this dependence without introducing a significant bias on the m_t measurement.

A. The Signal Likelihood

For the calculation of the signal likelihood, the procedure described in [8, 15] has been extended and optimized. It is based on the leading-order matrix element for the process $q\bar{q} \to t\bar{t}$ [16]. Aspects that are unchanged from [8, 15] are only briefly mentioned in the following. The matrix element for the process $gg \to t\bar{t}$ is not evaluated explicitly because the top and W propagator and decay parts of the matrix element, which contain most of the information on the top quark mass and the separation of signal and background events, are identical.

The correct association of reconstructed jets with the final-state quarks is not known. Therefore, the transfer function takes into account all possible jet-parton assignments as described in Section II C. For a given measured event x, the convolution integral in Equation (5) is calculated separately for each jet-parton assignment and for all different m_t assumptions, while all different S_b and S_l hypotheses are considered simultaneously. The integral evaluation is performed numerically with the Monte Carlo program VEGAS [17, 18], which has been slightly extended to achieve the simultaneous evaluation of several integrals with the same distribution of parton configurations y. A single call to the routine calculating the integrand returns an array of values for all assumed S_b and S_l values under consideration. This diminishes the total computation time spent for a given number of calls to evaluate the integrand, because the matrix element does not have to be re-evaluated when only the S_b or S_l assumptions change. Even more importantly, fluctuations between the results obtained for different S_b and S_l assumptions are reduced because the integrand is evaluated for the same parton configurations y.

While the expected measurement uncertainty on S_b and S_l is small relative to the resolution of jet energy measurements, the current uncertainty on the world average m_t value is of the same order as the top quark width. If the range of m_t hypotheses to be tested in a measurement spans a range of several times the top quark width, then the distribution of parton configurations y at which the integrand is evaluated for one m_t value is inappropriate for other values, and the technique becomes inefficient. Thus in the study presented here, the likelihoods for different m_t assumptions are evaluated independently.

To evaluate the signal likelihood for an event x and all assumed values of the quantities m_t, S_b, and S_l to be measured, the following computations are performed:

- Loop over all top quark mass assumptions,
- loop over all jet-parton assignments, and
- use the program VEGAS to compute the convolution integral in Equation (5) for all S_b and S_l hypotheses.

The integration in Equation (5) is over the kinematic variables of the assumed parton configuration, as described in Section II B. The number of dimensions is reduced by assuming perfect measurement of some of the quantities. Via variable transformation the remaining integration variables have been chosen such that where possible, they are uncorrelated, the integrand exhibits sharp peaks as a function of each individual variable (this optimizes the performance of the VEGAS program), and the variable transformation involves at most a quadratic equation (so the transformation is fast and numerically stable). The integration variables chosen in the lepton+jets and dilepton channels are summarized in Table II. The first two rows list variables corresponding to invariant masses and to jet momenta, respectively. Other variables are listed in the third row, and the final row indicates the integration necessary because of the finite muon momentum resolution.

The steps to evaluate the integrand for given values of the integration variables are:

- Determine the momenta of all final-state particles from the values of the integration variables.
- Evaluate the Jacobian determinant $\det(J)$ for the variable transformation.
- Calculate the value $|\mathcal{M}|^2 f_{\rm PDF}(\xi_1) f_{\rm PDF}(\xi_2)$ of the matrix element squared times PDF factors, summing over all possible initial-state parton species.
- Then loop over all final-state particles,
- for each particle, loop over all relevant S_b or S_l hypotheses, if applicable, and
- evaluate the transfer function factor corresponding to that particle.

lepton+jets channel	dilepton channel
$m^2_{t_1}$, $m^2_{t_2}$, $m^2_{W_{\rm had}}$	$m^2_{t_1}$, $m^2_{t_1}$
$\lvert\vec{p}_u\rvert$	$\lvert\vec{p}_{b_1}\rvert$, $\lvert\vec{p}_{b_2}\rvert$
$(\vec{p}_{b\nu})_z$	$(\vec{p}_{\nu_1}-\vec{p}_{\nu_2})_x$, $(\vec{p}_{\nu_1}-\vec{p}_{\nu_2})_y$
$(q/p_T)_\mu$	$(q/p_T)_\mu$

TABLE II: Overview of the integration variables for the signal likelihood calculation in the lepton+jets and dilepton channels. In the lepton+jets channel, the integration is over the masses of the two top quarks and the hadronically decaying W boson, the momentum of the up-type quark from the hadronically decaying W, and the sum of the longitudinal momenta of the b-quark from the top quark with the leptonic W decay and the neutrino. In the dilepton channel, the top quark masses, b-quark momenta, and the x and y components of the vectorial difference of the two neutrino momenta are taken as integration variables. The ratio of muon charge and transverse momentum is a further integration variable where applicable.

- Return the product

$$\begin{aligned} & \mathrm{d}\sigma_P(p\bar{p}\to y)\; W(x,y;\,S_b,S_l)\;\det(J) \\ = & \sum_{a_1,a_2} \mathrm{d}\xi_1\mathrm{d}\xi_2\; f^{a_1}_{\rm PDF}(\xi_1)\; \bar{f}^{a_2}_{\rm PDF}(\xi_2)\; \frac{(2\pi)^4\lvert\mathscr{M}_P\,(a_1a_2\to y)\rvert^2}{\xi_1\xi_2 s}\mathrm{d}\Phi_{n_f} \\ & \times W(x,y;\,S_b,S_l)\;\det(J) \end{aligned} \tag{20}$$

for all S_b and S_l hypotheses.

The convolution integral in Equation (5) has to be calculated for every selected event and is thus the most computing intensive part of the analysis. The optimization introduced here allows the integration necessary for the determination of three parameters in the lepton+jets channel to be performed within roughly the time needed in [8] for just two parameters.

The normalization $\sigma^{\rm obs\prime}_{t\bar{t}}$ only has to be determined once for a number of hypotheses relevant to the analysis. This is done in a separate program based on the VEGAS package that performs a 16-dimensional Monte Carlo integration over the observable final-state phase space. The phase space is generated recursively from the production of the $t\bar{t}$ pair and the subsequent two-body top and W decays.

B. The Background Likelihood

There are in general many background processes that can lead to an observed event. It is not problematic per se to not fully account for all backgrounds in the event likelihood. An incomplete background likelihood will lead to a shift of the measured top quark mass value (apart from an increased statistical uncertainty); the shift will in general depend on the top quark mass itself and on the fraction of events in the sample that are not accounted for in the overall likelihood. The shift is determined in the calibration procedure. When a background term is omitted in the event likelihood, the situation will thus be quantitatively, but not qualitatively different from that in an analysis that includes this term in the likelihood.

If several different background processes have similar kinematic characteristics, it is also possible to approximately describe the total background by the likelihood for only one of the background processes, multiplied by the total background fraction, cf. Equation (2). This technique has been applied by both CDF and D0 in the Matrix Element analyses in the lepton+jets channel, where a likelihood for QCD multijet production is not explicitly calculated.

Only leading-order background processes to $t\bar{t}$ events and only the most important ones among them are considered explicitly in this paper. To take into account all individual diagrams, routines from existing Monte Carlo generators are used to compute the likelihood for generic processes. They take into account the relative importance of the various subprocesses that contribute and perform a statistical sampling of all possible spin, flavor, and color configurations. Because the background likelihood does not depend on the top quark mass, it does not have to be computed for as many different assumptions as the signal likelihood and it is possible to evaluate the matrix element without a dedicated routine optimized for speed.

The generic background process taken into account in the lepton+jets channel is the production of a leptonically decaying W boson in association with four additional light partons, $Wjjjj$. Events with a leptonically decaying W boson and four partons that include heavy-flavor quarks are not considered separately because their kinematic characteristics are very similar to those of $Wjjjj$ events.

The VECBOS [19] generator is used to calculate the background likelihood L_{Wjjjj}. The jet directions and the charged lepton are taken as well-measured. The integral in Equation (5) is performed by generating Monte Carlo events with

quark energies distributed according to the jet transfer function. In these Monte Carlo events, the neutrino transverse momentum is given by the condition that the transverse momentum of the W+jets system be zero, while the invariant mass of the charged lepton and neutrino is assumed to be equal to the W mass to obtain the neutrino z momentum (both solutions are considered). All 24 possible assignments of jets to quarks in the matrix element are considered and their contributions to the likelihood summed. Monte Carlo events are drawn according to the appropriate jet resolution functions for the four reconstructed jets, the likelihood L_{Wjjjj} is computed for each of these events, and their mean value is used in the subsequent analysis. The study described in Section V supports that it is not necessary to compute the likelihood L_{Wjjjj} for different S_l values; only the value L_{Wjjjj} ($S_l = 1$) is used.

The measurement in the dilepton ($e\mu$) channel considers background from events containing a Z boson decaying via τ leptons to an electron and a muon (plus neutrinos) and two additional light partons explicitly in the event likelihood. The likelihood is calculated using the VECBOS generator as above, including the transfer function for leptonic τ decays described in Section II C. Again, the jet directions and the charged lepton are taken as well-measured, and the integral in Equation (5) is performed by generating Monte Carlo events with quark energies distributed according to the jet transfer function. The energies of the two τ leptons are then given by the condition that the transverse momentum of the Z+jets system be zero. Both possible assignments of jets to quarks are considered, and as above, only the value L_{Zjj} ($S_l = 1$) is used.

V. APPLICATION OF THE TECHNIQUE TO $t\bar{t}$ EVENTS IN THE LEPTON+JETS CHANNEL

The method is validated using smeared parton-level simulated $t\bar{t}$ and $Wjjjj$ events, generated as described in Section III. In this study, pool sizes of 1500 events for the lepton+jets $t\bar{t}$ signal process and 850 $Wjjjj$ background events are available. In order to model processes not covered by the method, two additional samples are generated. Out of the $Wjjjj$ background sample 450 events are modified into $Wb\bar{b}jj$ events by randomly assigning two light partons as b partons and smearing them according to the b quark transfer functions. With this sample, effects of heavy flavor content in the background can be studied. The other test sample is composed of 800 lepton+jets $t\bar{t}$ events that contain an additional parton from initial- or final-state radiation.

As the e+jets and μ+jets decay channels only differ in the momentum resolution of the lepton and whether a transfer function is used to parametrize it, no qualitative difference between measurements in the two channels is expected. This was verified in [20]. Thus, in the following only the e+jets decay channel will be considered. The different angular acceptance cuts for electrons and muons lead to different signal fractions for the two channels, but the conclusions from the studies described here are still valid since they have been performed for a wide range of signal fractions.

In Section V A the method is tested on ensembles containing signal events only. Section V B describes studies performed on samples including background events.

A. Signal-Only Studies

The method is first tested with ensembles only containing signal events. For these studies, 1000 pseudo-experiments are composed of 100 e+jets events each, and background likelihoods are not included. The reconstructed fit observables should resemble the generated input values within statistical uncertainties and the pull widths are expected to be equal to unity (within uncertainties).

The likelihood normalization $\sigma_{t\bar{t}}^{\mathrm{obs}\prime}$ as a function of the top quark mass as defined in Section II D is given in Figure 5 for the e+jets and μ+jets channels (only the e+jets function is further used). These functions are fitted with 3^{rd}-order polynomials as a function of the top quark mass. The two channels yield different normalization functions as the detector acceptance differs for the two lepton types.

In Figure 6, results for the measurements of the three fit observables m_t, S_b, and S_l can be found. In this and the similar figures that follow, the error bars represent the uncertainties arising from limited statistics in the ensemble tests. The reconstructed values reproduce the generated ones well, and the deviations between fitted and true values are adequately described by the fitted statistical uncertainties. The pull widths in Figure 6(d) are on average two standard deviations below the expectation. A similar conclusion cannot be drawn from Figures 6(e) and (f) since the same events are used for all S_b and S_l values except for a rescaling of jet energies. The results show that the method works in this test case and that the b-jet energy scale can be measured together with the top quark mass and light-jet energy scale.

In order to quantify the gain from the inclusion of b identification likelihoods as the factor W_b in Equation (13), the expected statistical uncertainties on the measurement quantities m_t, S_b, and S_l are depicted in Figure 7. These statistical uncertainties correspond to the hypothetical case of an integrated luminosity at the Tevatron of about

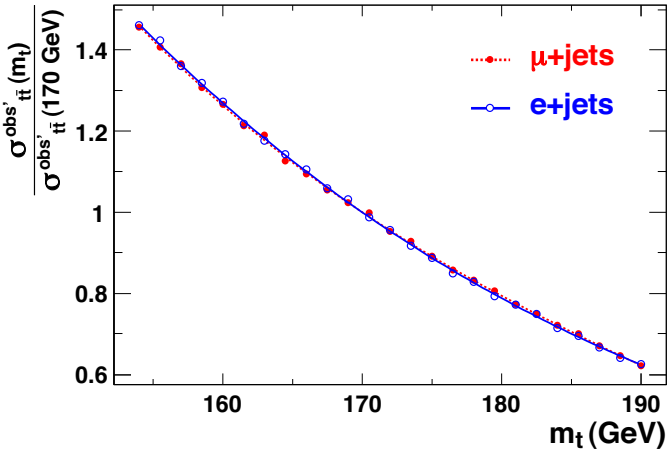

FIG. 5: Lepton+jets channel: Normalization function $\sigma_{t\bar{t}}^{\mathrm{obs}\prime}$ for the $t\bar{t}$ likelihood in the lepton+jets channel as a function of the top quark mass for the e+jets (blue) and μ+jets channels (red circles). The normalization functions are plotted relative to the fitted values for $m_t = 170\,\mathrm{GeV}$. An overall scale factor is irrelevant for the subsequent analysis because it is absorbed by the normalization procedure for the background likelihood.

0.8 fb^{-1} (for one experiment and one decay channel) without any background. The solid lines show the expected uncertainties obtained when using the full transfer function, while the uncertainties given by the dashed lines are obtained when the factor W_b is omitted from the transfer function. For all three quantities an improvement of about 15% on the expected relative statistical uncertainty can be achieved because of the additional b identification information. No systematic deviation between the measurement values obtained with and without b identification likelihoods is observed. The results without W_b are shown for illustration only; in the final studies with lepton+jets events the factor W_b is included.

B. Studies Including $Wjjjj$ and $Wb\bar{b}jj$ Background

For the background studies, ensembles are composed of 1000 pseudo-experiments with 200 events each, using different signal fractions. The case of a signal fraction $f_{t\bar{t}} = 50\,\%$ corresponds to an integrated luminosity at one Tevatron experiment of about 0.8 fb^{-1} (for one decay channel). Two sources of background are studied, $Wjjjj$ and $Wb\bar{b}jj$ events.

Background from $Wjjjj$ events, containing a leptonically decaying W and four light partons, is described by the background likelihood (see Section IV B) and thus accounted for. To study the dependence of the method on the background fraction, it is varied between 0% and 90% in 10% steps. Figure 8 shows the results for ensembles with true values of $m_t = 170\,\mathrm{GeV}$ and $S_b = S_l = 1$. The top quark mass fit yields the expected results even for background fractions significantly larger than those observed in the data. The two jet energy scales show deviations from the expected values when background is included; these deviations increase with the background fraction. This effect is not unexpected since the background likelihood is calculated only for the $S_b = S_l = 1$ hypothesis. However, this simplification is appropriate when the goal of the analysis is a measurement of the top quark mass, while the determination of the jet energy scales is only performed to reduce the systematic uncertainties on this measurement. The lack of an exact modelling of the jet energy scale in background events does not limit the precision of the top quark mass determination.

Background from W+jets events containing b quarks is topologically very similar to $Wjjjj$ background and is thus not treated as a separate process in the likelihood calculation. Nonetheless, if one includes b identification information in the analysis, $Wb\bar{b}jj$ events have to be considered carefully.

Figure 9 shows the difference between the log-likelihood values $\ln L_{t\bar{t}}$ and $\ln L_{Wjjjj}$ for $t\bar{t}$ signal as well as $Wjjjj$ and $Wb\bar{b}jj$ background events. The topological information alone already allows for a discrimination between signal and background. But as expected, there is no separation between background without ($Wjjjj$) and with ($Wb\bar{b}jj$) b jets; such a separation only arises when b identification information is included. Figure 9(a) is shown for illustration only; in the final studies with lepton+jets events the factor W_b is included in the transfer function as given in Equation (13).

Ensembles with $m_t = 170\,\mathrm{GeV}$ and $S_b = S_l = 1$ are created that have a fixed total fraction of background (50%), but the fraction of $Wb\bar{b}jj$ events within this background is varied. This means that an absolute fraction of $f_{Wb\bar{b}jj} = 0.5$

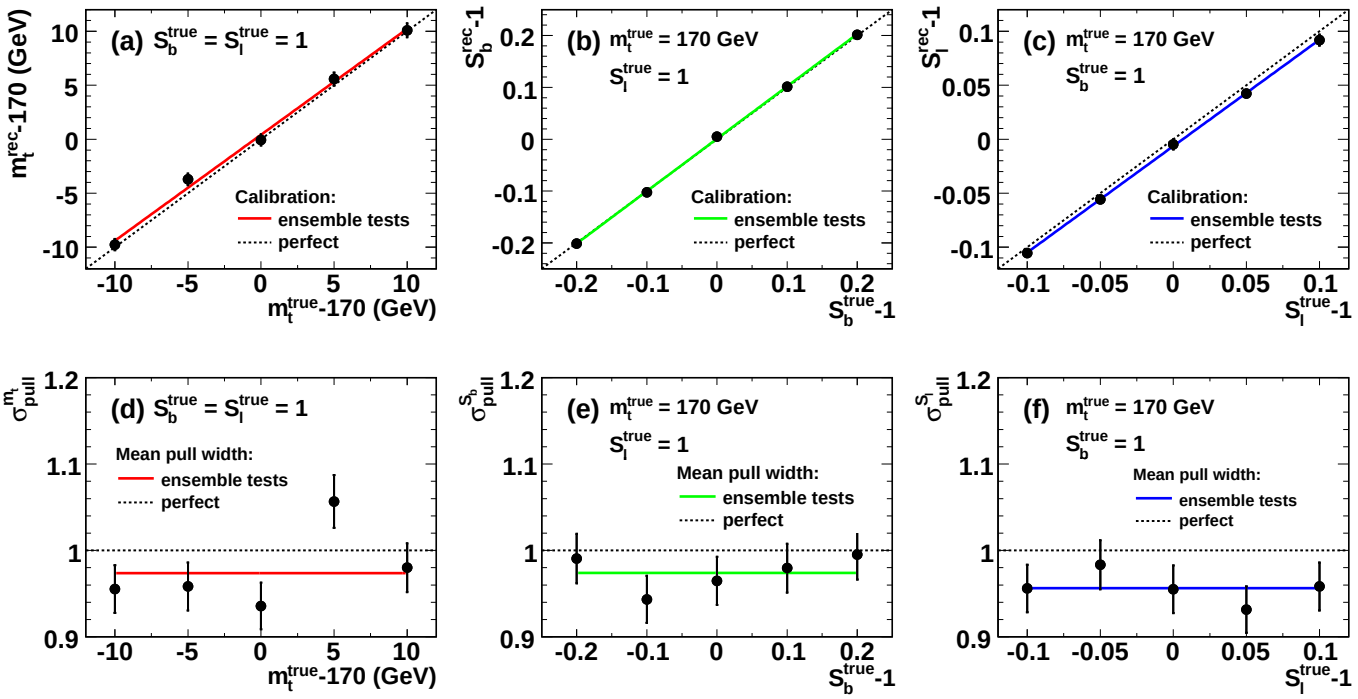

FIG. 6: Lepton+jets channel: Measurement of m_t, S_b, and S_l in pure signal ensembles. Reconstructed ("rec") vs. true values are shown in plots (a)-(c), the widths of the pull distributions vs. true values in plots (d)-(f). In plots (a)-(c) the solid lines show the results of straight-line fits, while in plots (d)-(f) they indicate the mean values. Event samples with the same m_t but different S_b or S_l values are correlated since they are obtained by scaling the final-state quark energies as described in Section III.

corresponds to pseudo-experiments in which the background consists solely of $Wb\bar{b}jj$ events. Figure 10 shows the results for the three measurement quantities versus the absolute fraction of $Wb\bar{b}jj$ events. The results indicate that there is only a weak dependence of the fit results on the fraction of $Wb\bar{b}jj$ events for all three fit observables. Consequently, only small systematic uncertainties arise in the calibration of the measurement, and it is justified that $Wb\bar{b}jj$ events are not accounted for explicitly in the event likelihood. Note that the results for $f_{Wb\bar{b}jj} = 0$ correspond to the values for $f_{Wjjjj} = 0.5$ in Figure 8 and that for S_b and S_l, deviations between fitted and true values are not unexpected for $f_{Wjjjj} > 0$ as explained above.

For an integrated luminosity of $12\,\text{fb}^{-1}$, a signal fraction $f_{t\bar{t}} = 50\,\%$, and absolute background fractions of $f_{Wjjjj} = 40\,\%$ and $f_{Wb\bar{b}jj} = 10\,\%$, the expected statistical uncertainties in the lepton+jets channel (combining the e+jets and μ+jets channels) obtained by a single Tevatron experiment are found to be

$$\begin{aligned} \sigma_{m_t}(\text{lepton+jets}) &= 0.45\ \text{GeV}\,, \\ \sigma_{S_b}(\text{lepton+jets}) &= 0.0064\,, \text{ and} \\ \sigma_{S_l}(\text{lepton+jets}) &= 0.0039\,. \end{aligned} \tag{21}$$

The slopes of the calibration curves are between 0.91 and 0.97 and have been accounted for, and the uncertainties have been multiplied with the pull widths between 0.94 and 1.04.

VI. APPLICATION OF THE TECHNIQUE TO $t\bar{t}$ EVENTS IN THE DILEPTON CHANNEL

This section describes the application of the Matrix Element method for a simultaneous measurement of the top quark mass and the b-jet energy scale in dilepton $t\bar{t}$ events in the $e\mu$ channel. As in the lepton+jets channel, to minimize computing time, the parton-level studies described here have been performed assuming perfectly measured lepton momenta, i.e. the generated leptons are not smeared, and the additional integration over the inverse muon transverse momentum is not carried out. This approach is valid here because the aim is to study the behavior of

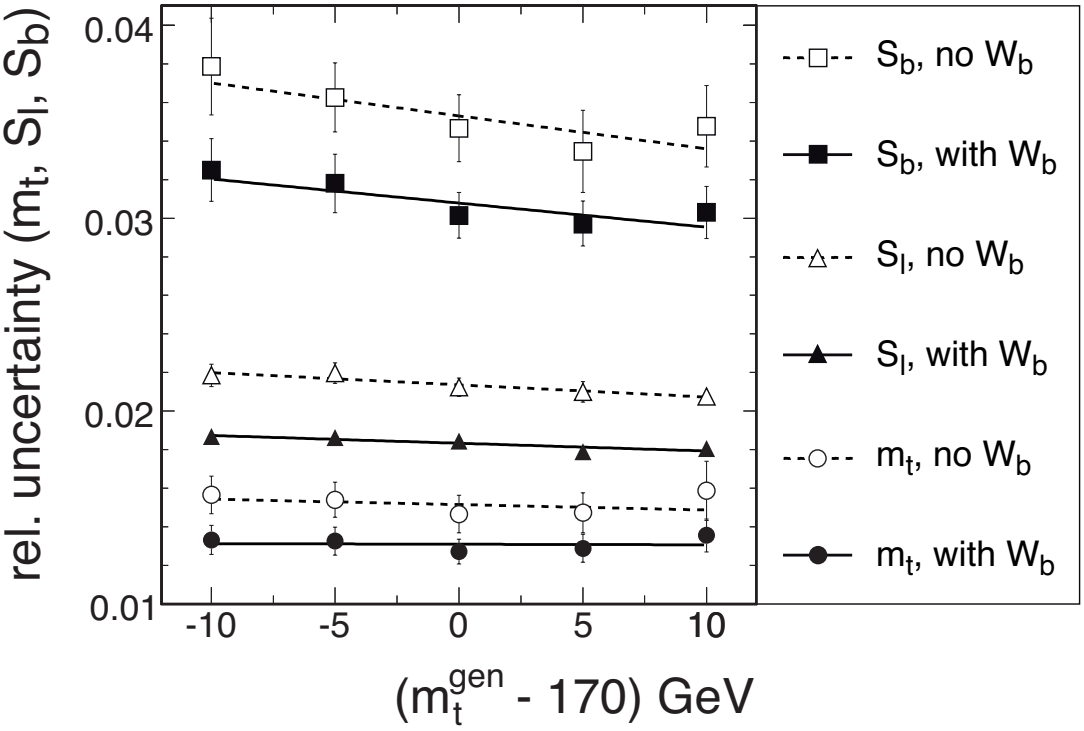

FIG. 7: Lepton+jets channel: Expected statistical uncertainties of the m_t (circles), S_b (squares), and S_l (triangles) determination in pseudo-experiments with signal events only. The filled markers are the results with the full transfer function included, whereas the open markers lack the W_b factor (b identification). Solid and dashed lines indicate straight-line fits to the points.

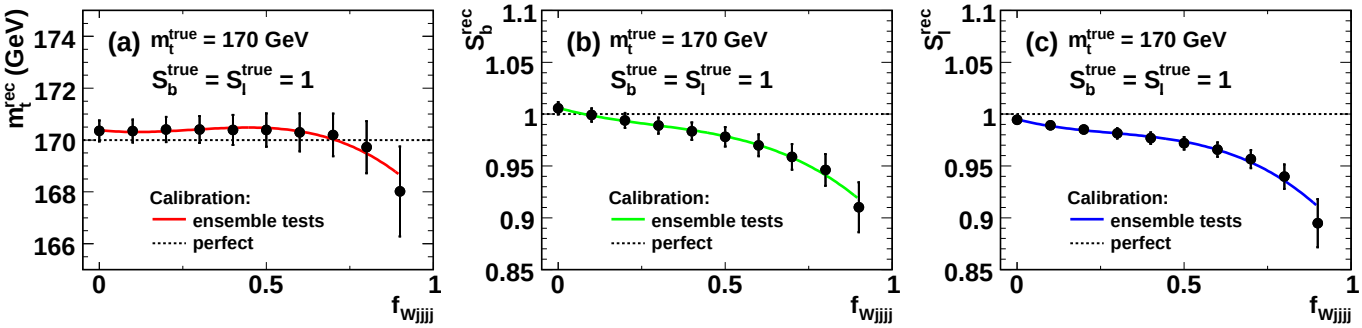

FIG. 8: Lepton+jets channel: Measurement of (a) m_t, (b) S_b, and (c) S_l in ensembles including $Wjjjj$ background. Reconstructed values are shown as a function of the background fraction. The individual points in each plot are correlated because the ensembles are drawn from the same event pools. The lines indicate the results of 3^{rd}-order polynomial fits to the points.

the measurement method when applied to pseudo-experiments with different background compositions, and because it has been verified that the conclusion from the parton-level tests stays the same and is not affected by this choice. To validate the integration over the inverse muon momentum, an additional test has been performed using smeared leptons [21].

In the dilepton channel, b-tagging information cannot help to select the correct assignment of jets to partons as in the lepton+jets case (except in events with significant gluon radiation). Since the background to $t\bar{t}$ dilepton events is small, no b-tagging information has been used in the studies shown in this section, i.e. the factor W_b has been omitted from the transfer function in Equation (13).

As the missing transverse momentum $\not\!\!E_T$ depends on the reconstructed jet energies, the normalization of the signal likelihood depends not only on m_t, but also on S_b. For a given value of S_b, the normalization is calculated as a

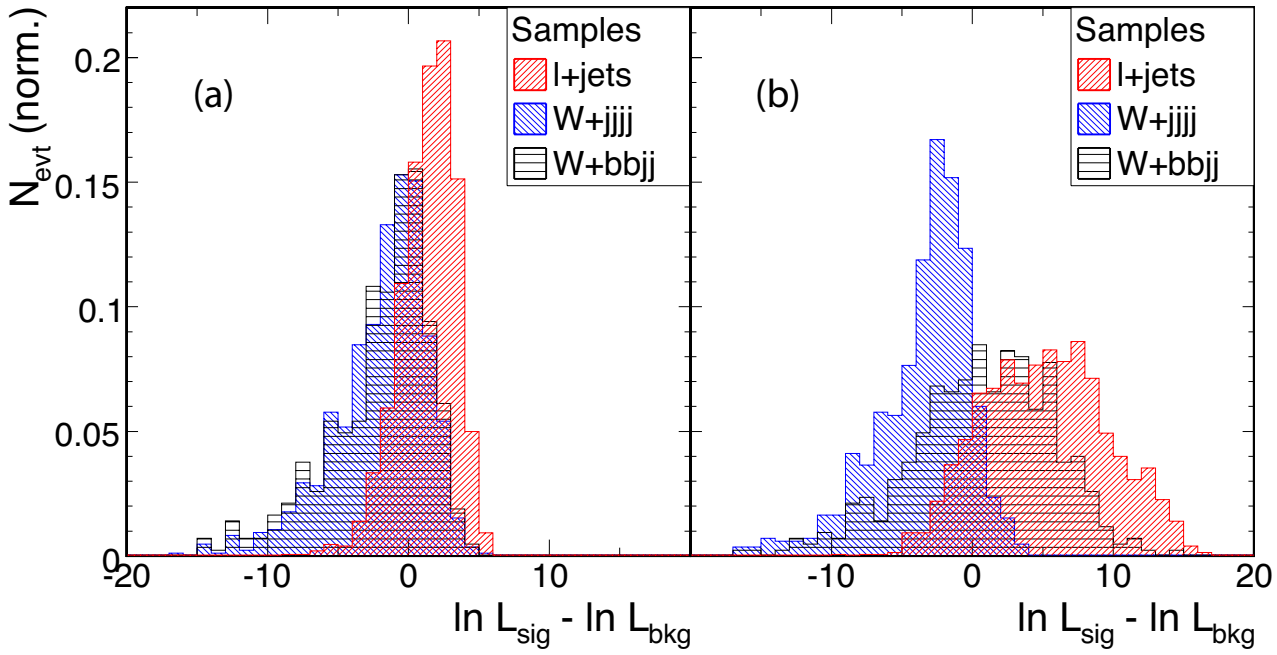

FIG. 9: Lepton+jets channel: Difference between the log-likelihood values $\ln L_{t\bar{t}}$ and $\ln L_{Wjjjj}$ for lepton+jets $t\bar{t}$ signal as well as $Wjjjj$ and $Wb\bar{b}jj$ background events. Each individual distribution is normalized. In plot (a), the W_b factor has been omitted in the transfer function, while it is included in plot (b).

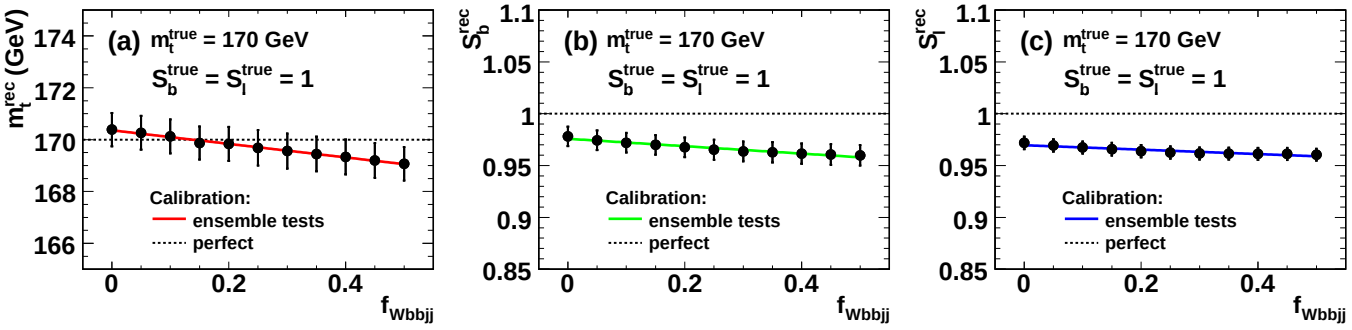

FIG. 10: Lepton+jets channel: Measurement of (a) m_t, (b) S_b, and (c) S_l in ensembles including $Wjjjj$ and $Wb\bar{b}jj$ background. Reconstructed values are shown vs. the absolute $Wb\bar{b}jj$ background fraction. The total fraction of background is fixed to 50%. The uncertainties on the individual points are correlated. The lines indicate the results of straight-line fits to the points.

function of the top quark mass and fitted with a 3^{rd}-order polynomial, similar to what is shown in Figure 5. Each of the four parameters of the polynomials as a function of S_b are then fitted in turn with a quadratic function. The resulting two-dimensional normalization is shown in Figure 11. The relative normalization of the background and signal likelihoods is derived as described in Section II D 5.

Similar to Section V, ensemble tests under different hypotheses are described in the following.

A. Signal-Only Studies

In a first step, ensemble tests with pure signal events are performed, and the signal likelihood is taken as the event likelihood. For each of nine calibration points in the (m_t, S_b) plane, 1000 pseudo-experiments are performed. Each of the pseudo-experiments is built of 50 $t\bar{t}$ events in the $e\mu$ channel, corresponding to an integrated luminosity of

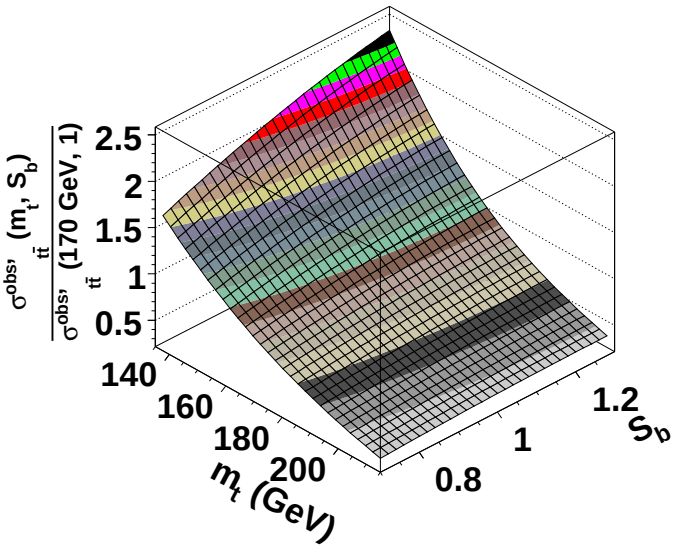

FIG. 11: Dilepton channel: Normalization function $\sigma_{t\bar{t}}^{\mathrm{obs}\prime}$ for the $t\bar{t}$ likelihood in the dilepton channel as a function of the top quark mass and b-jet energy scale, normalized to the fitted value for $m_t = 170\,\mathrm{GeV}$ and $S_b = 1$.

about 1.4 fb^{-1} at the Tevatron [22]. At all calibration points, the generated and the measured values of the top quark mass and b-jet energy scale are in excellent agreement. The uncertainty on m_t (S_b) does not depend on S_b (m_t), and increases with m_t (S_b) as expected. The pull width is always consistent with unity within uncertainties.

B. Studies Including $Z/\gamma^*(\to \tau^+\tau^-)jj$ and $Z/\gamma^*(\to \tau^+\tau^-)b\bar{b}$ Background

In the next step, the dominant source of background is added, i.e. $Z/\gamma^*(\to \tau^+\tau^-)jj$ events where the Z boson decays into an electron and a muon via two τ leptons. Accordingly, the $Z/\gamma^*(\to \tau^+\tau^-)jj$ likelihood is included in the event likelihood.

In each of the 1000 pseudo-experiments, 50 events are used, and the fraction of $Z/\gamma^*(\to \tau^+\tau^-)jj$ events is varied from 10% to 50% in steps of 10%. Within statistical uncertainties, the measured values of m_t and S_b do not depend on the fraction of $Z/\gamma^*(\to \tau^+\tau^-)jj$ events. Figure 12 shows the calibration curves for m_t and S_b for pseudo-experiments containing 30% of $Z/\gamma^*(\to \tau^+\tau^-)jj$ events. This fraction corresponds roughly to the total fraction of background events selected by the D0 experiment in the $e\mu$ channel [22]. Both calibration curves are in excellent agreement with the expectation. The pull widths of the m_t and S_b measurements are consistent with unity for all ensembles.

To study the effect of jets from b quarks, $Z/\gamma^*(\to \tau^+\tau^-)b\bar{b}$ events are also included in the pseudo-experiments. These are described by the $Z/\gamma^*(\to \tau^+\tau^-)jj$ likelihood; no dedicated likelihood for $Z/\gamma^*(\to \tau^+\tau^-)b\bar{b}$ events is included. The sum of the fractions of $Z/\gamma^*(\to \tau^+\tau^-)jj$ and $Z/\gamma^*(\to \tau^+\tau^-)b\bar{b}$ events is kept at 30%, and the absolute contribution from $Z/\gamma^*(\to \tau^+\tau^-)b\bar{b}$ is varied between 3% and 15% in steps of 3%. Within statistical uncertainties, no effect from the jet flavor can be observed on the mean expected measurement values or the widths of the pull distributions.

C. Studies Including $Z/\gamma^*(\to \tau^+\tau^-)jj$ and $WWjj$ Events

Additional contamination of the selected dilepton data sample comes from $WWjj$ events. The expected fraction in the $e\mu$ channel compared to $Z/\gamma^*(\to \tau^+\tau^-)jj$ events is about one fourth [22]. A study has been performed where each of the 1000 pseudo-experiments is composed on average of 35 signal, 12 $Z/\gamma^*(\to \tau^+\tau^-)jj$, and 3 $WWjj$ events. The $WWjj$ events are not described by a dedicated likelihood because their contribution to the event sample is small.

Figure 13 shows the calibration curves of the top quark mass and the b-jet energy scale. Their slopes degrade slightly to $92 \pm 6\%$ and $94 \pm 4\%$, respectively. The pull widths increase to 1.06 ± 0.01 and 1.08 ± 0.01. In a measurement, the

fitted values have to be adjusted according to the calibration curve, and the S_b uncertainty has to be scaled by the pull width.

Note that in this case it is not expected to obtain perfect calibration curves, because the $WWjj$ background is not described with a separate likelihood. This study shows that it is possible to perform the measurement even when a background source is not accounted for in the likelihood.

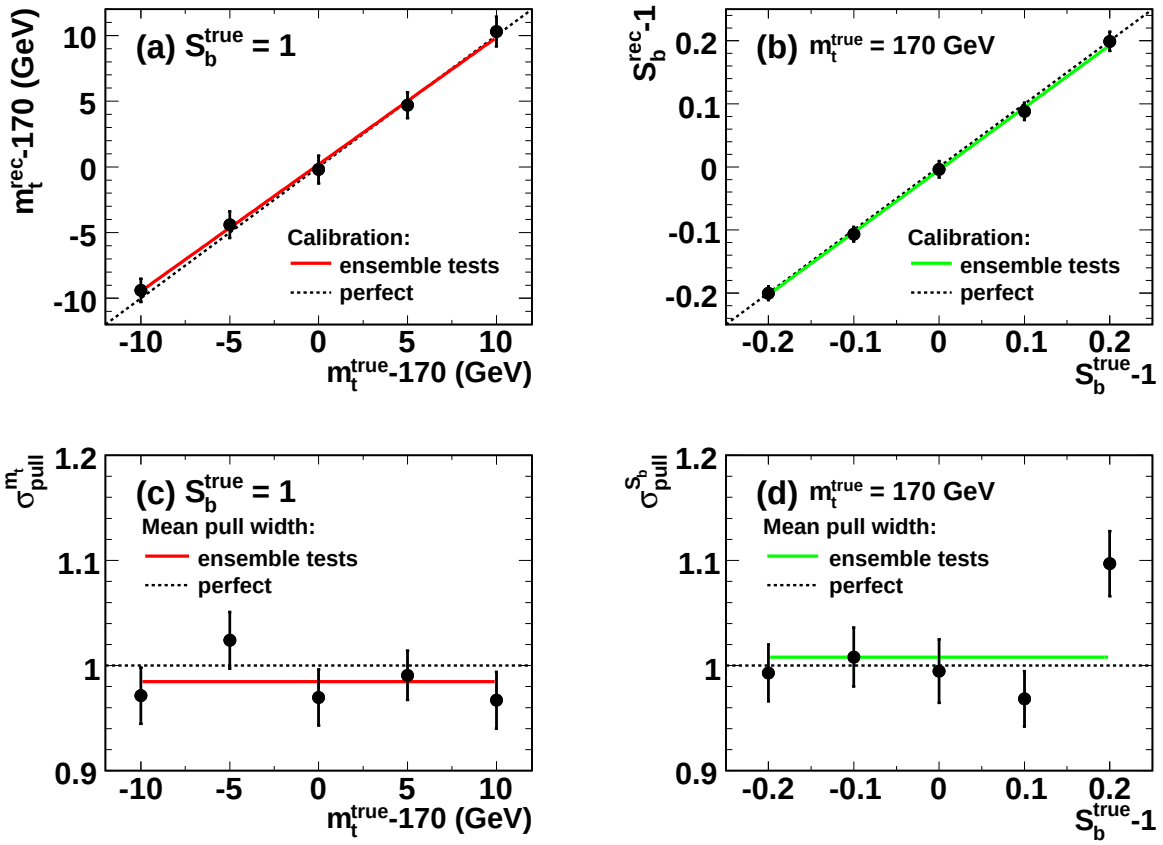

FIG. 12: Dilepton channel: Measurement of m_t and S_b in ensembles including 30% of $Z/\gamma^*(\to \tau^+\tau^-)jj$ background. Reconstructed ("rec") vs. true values are shown in plots (a) and (b), pull widths vs. true values in plots (c)-(d). In plots (a) and (b) the lines show the results of straight-line fits, while in plots (c) and (d) they indicate the mean values.

For an integrated luminosity of $12\,\text{fb}^{-1}$, a signal fraction $f_{t\bar{t}} = 70\,\%$, and absolute background fractions of $f_{Z/\gamma^*(\to\tau^+\tau^-)jj} = 24\,\%$ and $f_{WWjj} = 6\,\%$, the expected statistical uncertainties in the $e\mu$ channel obtained by a single Tevatron experiment are found to be

$$\begin{aligned} \sigma_{m_t}(e\mu) &= 2.3 \text{ GeV and} \\ \sigma_{S_b}(e\mu) &= 0.028\,. \end{aligned} \tag{22}$$

The slopes of the calibration curves in Figures 13(a) and (b) have been accounted for, and the uncertainties have been multiplied with the pull widths shown in Figures 13(c) and (d). The statistical correlation between the m_t and S_b measurements is $-55\,\%$.

VII. SYSTEMATIC UNCERTAINTIES

For a measurement, uncertainties in the properties of the full simulation (a GEANT-based detector simulation for all relevant processes) used for the calibration have to be accounted for by systematic uncertainties on the measurement result. These systematic uncertainties are not necessarily equal in magnitude to the corrections derived in the calibration. Systematic uncertainties arise from three sources: modeling of the detector performance, uncertainties in the method itself, and modeling of the physics processes for $t\bar{t}$ production and background.

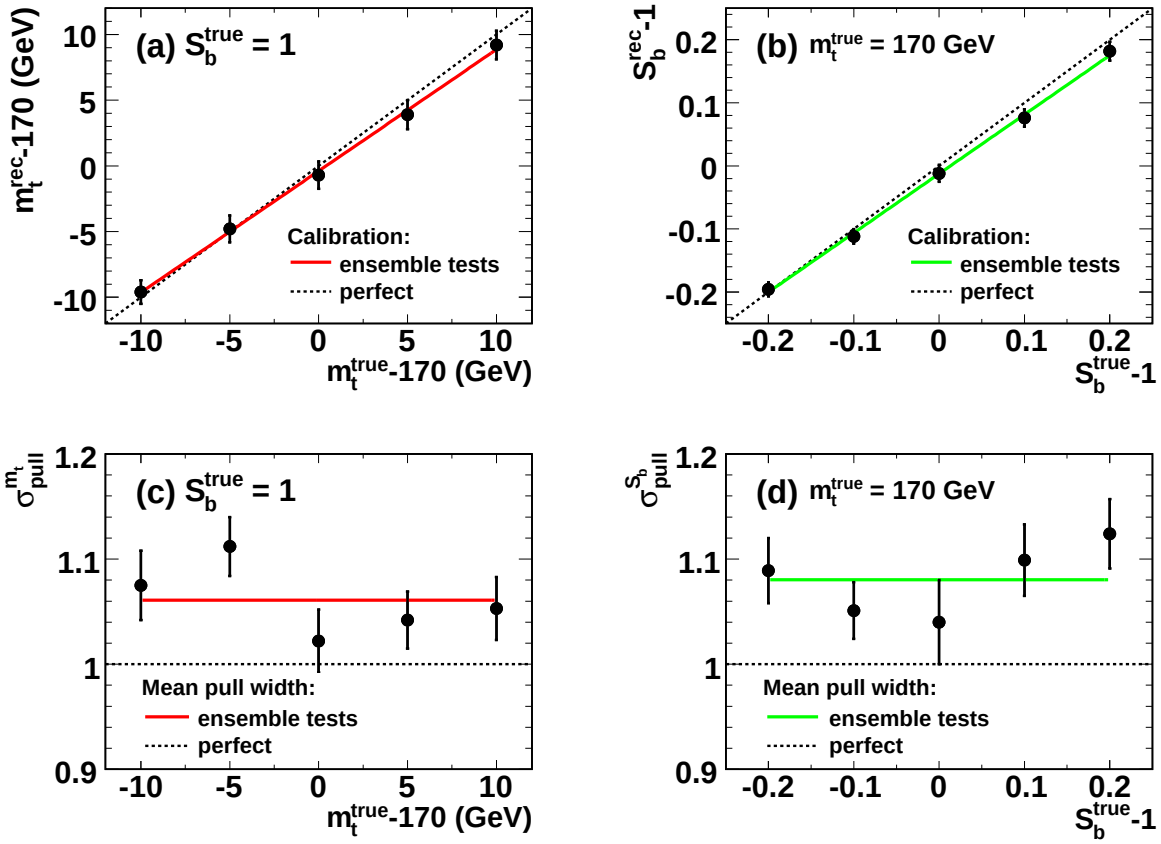

FIG. 13: Dilepton channel: Measurement of m_t and S_b in ensembles including 24% of $Z/\gamma^*(\rightarrow \tau^+\tau^-)jj$ and 6% of $WWjj$ background. Reconstructed ("rec") vs. true values are shown in plots (a) and (b), pull widths vs. true values in plots (c)-(d). In plots (a) and (b) the lines show the results of straight-line fits, while in plots (c) and (d) they indicate the mean values.

In the first top quark mass measurements, the largest systematic uncertainties related to the detector performance originated from the absolute jet energy scales S_b and S_l. With the technique described in this paper, these uncertainties can be absorbed into the statistical uncertainty. Uncertainties on the top quark mass due to the $|\eta|$ or energy dependencies of the jet energy scales or due to other detector effects like energy dependent efficiencies are typically much smaller.

An uncertainty arises from the finite event samples used to calibrate the method, which is reflected in uncertainties on the calibration curves shown e.g. in Figures 6 and 13. These uncertainties can be reduced when larger simulated event samples are used. Since all other effects are accounted for by the uncertainties on the properties of the full simulation used in the calibration, no additional uncertainties are assigned to the measurement method itself.

A significant systematic uncertainty in previous top quark mass measurements was due to the uncertainty in modeling of initial- and final-state gluon radiation. The most basic uncertainty is related to the overall fraction of events with significant radiation. Since the jet energy scales are measured from the data, it can be expected that the method is insensitive to the amount of (soft) gluon radiation off the final-state quarks, while knowledge of the amount of initial-state radiation is important. Dedicated ensemble tests to study events with significant radiation have been performed and are described in the following section.

A. Studies of $t\bar{t}$ Events with Initial- and Final-State Radiation

The model described so far does not account for $t\bar{t}$ events with an additional hard parton from initial- or final-state radiation ($t\bar{t}j$). When the $t\bar{t}$ events are replaced by such $t\bar{t}j$ events, ensemble tests yield deviations of about 4 GeV from the nominal top quark mass in both the lepton+jets and dilepton channels. Thus, the method presented so far relies on the knowledge of $f_{t\bar{t}j}$, and an uncertainty on $f_{t\bar{t}j}$ directly translates into an uncertainty on the top quark

mass.

An ensemble test has been performed with $t\bar{t}j$ events using an extended model, which has first been described in [21]. The assumption of zero transverse momentum of the $t\bar{t}$ system is dropped, an additional integration over the two transverse momentum components of the $t\bar{t}$ system is performed in the likelihood calculation, and an additional factor $W_{p_{T,t\bar{t}}}$ is introduced which describes the likelihood to obtain a $t\bar{t}$ system with a given transverse momentum. The ensemble test is performed with pseudo-experiments containing 50 dilepton $t\bar{t}j$ signal events. The true top quark mass is 170 GeV and the true b-jet energy scale is 1.0. Figure 14 shows the results of this ensemble test which yields expected central measurement values for the top quark mass of 170.6 ± 1.0 GeV and for the b-jet energy scale of 1.004 ± 0.013, consistent within uncertainties with the input values. The pull widths are consistent with 1.0 in both cases.

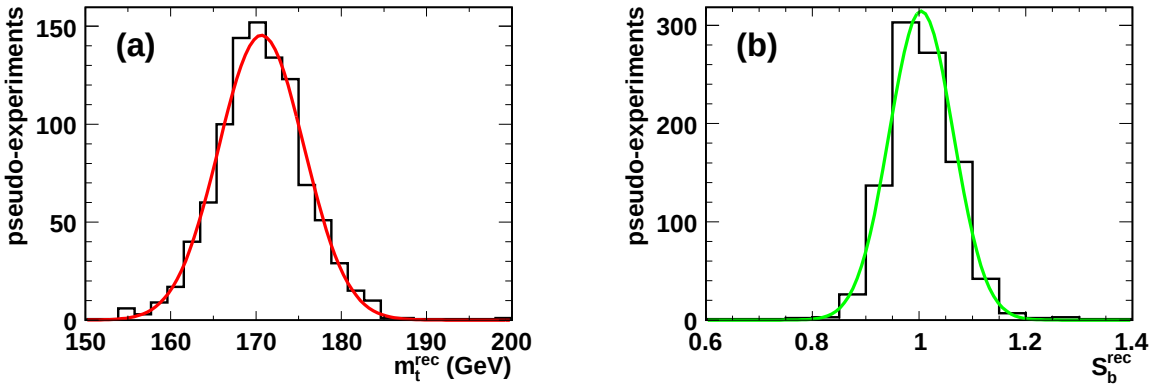

FIG. 14: Dilepton channel: Measurement of m_t and S_b in pseudo-experiments of 50 dilepton $t\bar{t}$ signal events with non-zero $t\bar{t}$ transverse momentum. True values of $m_t = 170$ GeV and $S_b = 1.0$ were used. Shown are the distributions of (a) the reconstructed top quark mass and (b) the reconstructed b-jet energy scale.

This test shows that it is possible to adequatly describe $t\bar{t}j$ events in the method. To reduce the systematic error on the top quark mass that arises from the uncertainty on the fraction of $t\bar{t}j$ events in the data sample, the method should be extended in the future by introducing the fraction of such events as an additional unknown parameter to be measured from the data, similar to the parameters S_b and S_l.

VIII. CONCLUSIONS

The Matrix Element method is a powerful analysis tool that has been applied with great success in measurements of the top quark mass, the discovery of electroweak single top quark production, and searches for the Higgs boson. In this paper, a detailed introduction into the method is given with the aim of facilitating its application to further measurements. The principle of the method is introduced, and details concerning the description of the detector response are given.

It has been proposed previously to overcome the current limitation in top quark mass measurements arising from experimental systematic uncertainties by a simultaneous determination of the top quark mass as well as the absolute energy scales for both b-quark and light-quark jets. The paper discusses how this strategy can be implemented naturally in the Matrix Element method for measurements in both lepton+jets and dilepton events at hadron colliders. It is shown that the limiting systematic uncertainty in current measurements (arising from the absolute energy scale for b-quark jets) can be overcome. In the future, it should be possible to render the method stable also against systematic uncertainties related to the fraction of events with significant initial- or final-state radiation.

In conclusion, we have given a general introduction to the Matrix Element method, and we have shown how future measurements of the top quark mass can be performed with the Matrix Element method in order to reduce the experimental systematic error.

Acknowledgements

The authors would like to thank Gaston Gutierrez and Juan Estrada for their fundamental contributions to the development of the Matrix Element method, many of which are part of the foundation for the work presented here. Also, the authors would like to thank Raimund Ströhmer for his careful reading of the manuscript and his very valuable comments, and all their colleagues at the Tevatron experiments D0 and CDF for many helpful discussions. All authors have previously been employed at Munich University (LMU), where a substantial part of the work towards this paper has been performed, and would like to thank Dorothee Schaile, Otmar Biebel, and all members of the LMU experimental particle physics group.

---

[1] V. M. Abazov *et al.*, Nature **429** (2004) 638;
V. M. Abazov *et al.*, Phys. Lett. B **617** (2005) 1;
K. Kondo, J. Phys. Soc. Jpn. **60** (1991) 836;
R. H. Dalitz and G. R. Goldstein, Phys. Rev. D **45** (1992) 1531.
[2] A. Abulencia *et al.*, Phys. Rev. Lett. **99** (2007) 182002;
T. Aaltonen *et al.*, Phys. Rev. Lett. **102** (2009) 152001;
V. M. Abazov *et al.*, Phys. Rev. Lett. **101** (2008) 182001.
[3] V. M. Abazov *et al.*, Phys. Rev. Lett. **103** (2009) 092001;
T. Aaltonen *et al.*, arXiv:1004.1181 [hep-ex] (2010).
[4] F. Fiedler, habilitation thesis at Munich University (2007), arXiv:1003.0521.
[5] F. Fiedler, Eur. Phys. J. C **53** (2008) 41.
[6] C. Amsler *et al.*, Phys. Lett. B **667** (2008) 1, and 2009 partial update for the 2010 edition.
[7] R. Brun and F. Carminati, CERN Programming Library Long Writeup **W5013** (1993).
[8] V. M. Abazov *et al.*, Phys. Rev. D **74** (2006) 092005.
[9] T. Aaltonen *et al.*, Phys. Rev. D **79** (2009) 072001.
[10] V. M. Abazov *et al.*, Phys. Rev. D **75** (2007) 092007.
[11] R. Barlow, "Application of the bootstrap resampling technique to particle physics experiments," MAN/HEP/99/4 (2000), `http://www.hep.man.ac.uk/preprints/manhep99-4.ps`
[12] F. Maltoni and T. Stelzer, JHEP **0302** (2003) 027.
[13] M. L. Mangano, M. Moretti, F. Piccinini, R. Pittau and A. D. Polosa, JHEP **0307** (2003) 001.
[14] H. L. Lai *et al.*, Eur. Phys. J. C **12** (2000) 375.
[15] P. Schieferdecker, PhD thesis at Munich University (2005), FERMILAB-THESIS-2005-46.
[16] G. Mahlon and S. J. Parke, Phys. Lett. B **411** (1997) 173.
[17] G. P. Lepage, J. Comput. Phys. **27** (1978) 192.
[18] G. P. Lepage, Cornell preprint CLNS:80-447 (1980).
[19] F. A. Berends, H. Kuijf, B. Tausk and W. T. Giele, Nucl. Phys. B **357** (1991) 32.
[20] P. Haefner, PhD thesis at Munich University (2008), FERMILAB-THESIS-2008-51.
[21] A. Grohsjean, PhD thesis at Munich University (2008), FERMILAB-THESIS-2008-92.
[22] V. M. Abazov *et al.*, Phys. Lett. B **679** (2009) 177.